Power and loads for wind turbines in yawed conditions

Analysis of field measurements and aerodynamic predictions

K. Boorsma

November 2012
ECN-E--12-047

Abstract

This report gives a description of the work done within the framework of the FLOW project on single turbine performance in yawed flow conditions. Hereto both field measurements as well as calculations with an aerodynamic code are analyzed.

Acknowledgement
This work is subsidized by the FLOW programme under project number 5.1440. Leo Machielse is acknowledged for providing his analysis of the measured field data. Gerard Schepers, Koert Lindenburg and Arno vd Werff are acknowledged for their assistance during interpretation of the results.

Contents

List of Figures

List of Tables

1

Introduction

The rotors of horizontal axis wind turbines follow the changes in the wind direction for optimal performance. The reason is that the power is expected to decrease for badly oriented rotors. So, insight in the effects of the yaw angle on performance is important for optimization of the yaw control of each individual turbine.

The effect of misalignment on performance and loads of a single 2.5 MW wind turbine during normal operation is investigated. Hereto measurements at the ECN Wind Turbine Test Site Wieringermeer (EWTW) are analyzed from December 2004 until April 2009. These field measurements have been analyzed before in [14, 15]. In addition to that the influence of yaw is studied using a design code and results from this design code are compared with wind tunnel measurements.

2

Field measurements

The EWTW farm [7] consists of a row of five 2500 kW turbines with variable speed-pitch regulated control. These turbines have a diameter and a hub height of 80 m and are placed at mutual distances of 3.8 rotor diameters. The EWTW farm is very well suited for investigation into effects at full scale because of its state of the art turbines and the comprehensive and reliable measurement infrastructure for turbine and meteorological data.

The farm is orientated from west to east (95° - 275°), Figure 2.1. Turbine 5 is used for the power analysis in this report as this turbine is exposed to the prevailing westerly winds. Turbine 6 has been instrumented with blade root strain gauges and hence is used for the loads analysis. In addition to that a variety of signals is measured on all turbines, including electric power, nacelle wind speed and direction (both absolute nacelle direction as well as the direction of the wind vane), rotor speed and blade pitch angle. The wind characteristics are measured with the meteorological tower at 3.5D distance south-east of turbine 5 and 2.5D south-west of turbine 6. This mast measures wind speed and direction at three different heights including hub height. Also air pressure and temperature are measured at this height. The measurements at the EWTW are analyzed from December 2004 until April 2009.

2.1 Data reduction

2-, 5- and 10-minute statistics have been retrieved from the data base. The 2-minute SQL-scripts for this purpose can be found in appendix A. Wind direction, operational mode and minimum power are used as filter criteria in these scripts.

After retrieving the statistics from the database, a second data reduction step is performed to filter out erroneous samples and outliers. These steps are outlined in the sections on Turbine 5 and 6 below.

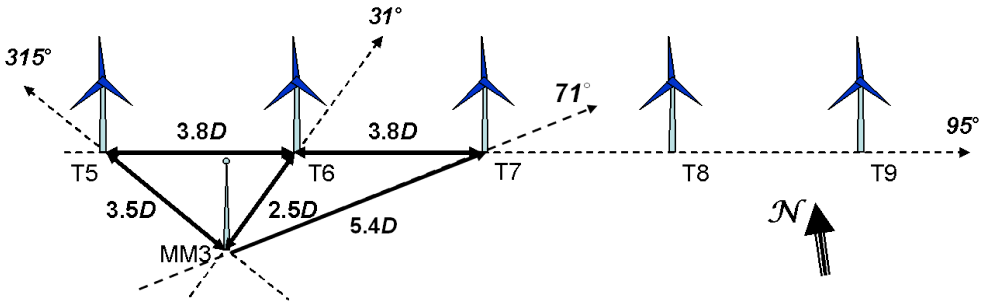

Figure 2.1: Main dimensions and directions in the EWTW farm. T5 to T9 are the turbine positions, MM3 indicates the measurement mast.

Bin averaging Bin averaging is applied to the resulting data sets both in wind speed and misalignment direction. The bin averaging settings are given in Table 2.1. The standard error of the mean within each bin is calculated using

$$S = \sigma/\sqrt{N} \quad , \tag{2.1}$$

with

S	[]	standard error of bin average mean
σ	[]	standard deviation of the bin data samples
N	[-]	number of samples per bin

Table 2.1: Bin averaging settings

	2 min average	5 min average	10 min average
Required samples per bin for valid average	25	12	8
Wind speed bins	5 to 13 m/s, Δ= 1 m/s		
Misalignment bins	-30° to 30°, Δ= 5 °		

Curve fitting The available power data have been curve fitted per wind speed bin using the available data points within each bin. The following equation is used

$$Cp = Cp_0 \cos^{\beta}(\phi - \phi_0) \quad , \tag{2.2}$$

with

Cp	[-]	power coefficient (equation 2.3)
Cp_0	[-]	maximum power coefficient (zero misalignment)
β	[-]	power exponent
ϕ	[°]	yaw angle
ϕ_0	[°]	yaw angle at Cp_0.

Although there is no solid physical background behind the assumed cosine dependence, previous research on this subject [6] has indicated this relationship to yield a good fit. Using a least squares estimate, Cp_0 and β are fitted. The value of ϕ_0 is fixed depending on the data set.

Turbine 5

The data reduction procedure is given below. For more details, please consult appendix B.1 which contains a summary of the results of this procedure.

Non-numeric values The misalignment of the turbine is calculated by means of subtracting the average wind direction measured by the meteo mast from the average nacelle direction. In some cases the nacelle direction is not recorded, resulting in a non-numeric value (NaN). These values are excluded from the dataset. The same holds for samples with NaN values of air pressure ('Pair').

Controller update As concluded in [15] and depicted in Figure 2.2a, a step or shift in the misalignment angle has been observed. This was most probably caused by a control update by the turbine manufacturer [10], causing an abrupt change in the nacelle direction. This splits the data set in two parts. Set 1 is roughly dated between December 2004 and July 2007 and set 2 roughly between September 2007 and March 2009. Unfortunately the exact offset between the datasets is unknown, which makes it impossible to merge them.

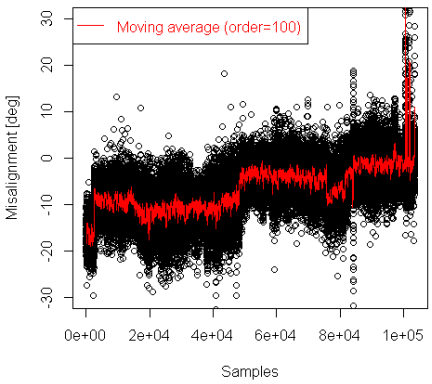

(a) Misalignment values as a function of chronologically taken samples

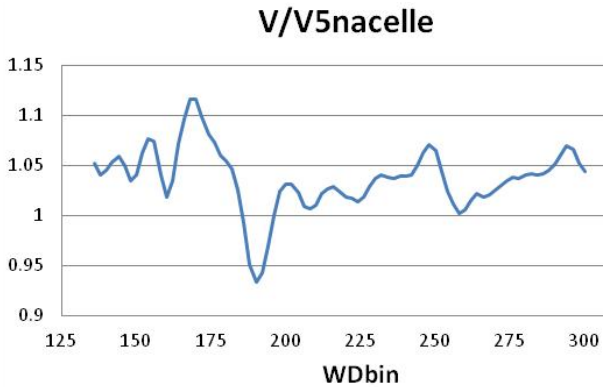

(b) Ratio of meteo mast measured wind speed over nacelle wind speed as a function of wind direction

Figure 2.2: Data reduction figures for Turbine 5

In addition to the jump, it can be observed that the calculated average misalignment is not, as expected, at zero degrees. This gives rise to the expectation that the absolute nacelle direction signal is not calibrated or the turbine is operating at yawed conditions. It should be noted that the yaw control of the turbine is not determined using the meteo mast wind direction. The manufacturer has indicated that indeed the absolute nacelle direction signal is not calibrated and is not used for controlling the turbine. Unfortunately the nacelle wind vane signal is unsuitable for a further check since it is influenced by the rotational flow of the rotor.

Wind direction Not all wind directions are suited for the analysis because of possible disturbances by the surrounding turbines on the performance of the turbines and/or on the wind speed measurement in the meteo mast MM3 which is located at 2.5 or 3.5 diameters distance in south-west direction.

Figure 2.2b shows the ratio of the wind speed measured by the meteo mast and the wind speed measured at the nacelle for wind directions between 135° and 300°. Rather big disturbances can be observed from wind directions up to 200°. From [17] it can be concluded that these disturbances are originated mainly by the NM52 turbine south of the farm and by the prototype turbines of the EWTW. Therefore only wind directions between 200° and 300° are considered for turbine 5.

Power and operational mode Only normal operation conditions below rated wind speed are considered. This is done by restricting the ”op_mode” signal between 11.0 and 11.2. In addition to that the minimum average power is set to 25 kW.

Nacelle direction standard deviation The standard deviation of the nacelle direction indicates to what extent the turbine has been yawing during the sample. Samples have been excluded for standard deviation exceeding 1°.

Average wind speed Although operational mode and minimum power filters should have excluded unsuitable samples, the average wind speed has also been restricted between 5 and 13 m/s.

Nacelle to wind speed ratio The wind speed is measured at the meteo mast located 3.5 diameters distance from the turbine. There can be differences between the wind that is experienced by the turbine and the meteo mast. Since the wind speed at the meteo mast is used to correlate with the turbine measurements, ratios between average nacelle and wind speed are restricted between 0.9 and 1.1.

Average pitch angle and variation Even during normal operation pitch angles can vary. The standard pitch angle for both data set 1 and 2 amounts to 0.065°. The sample average is allowed to deviate 0.05° above and below this value. In addition to the average, the difference between the maximum and minimum pitch angle of a data set is restricted to 0.05°.

Turbulence intensity The turbulence intensity can be calculated by dividing the standard deviation of the wind speed over its average, both measured at the meteo mast. Extremely low and high values are filtered out by restricting this value between 1% and 20%

Correction for atmospheric conditions The power coefficient can be defined as

$$Cp = P/(0.5\rho U^3 A) \quad , \tag{2.3}$$

with

Cp	[-]	power coefficient
P	[Watt]	electric power
ρ	[kgm^{-3}]	air density
U	[m/s]	wind speed
A	[m^2]	rotor area.

The air density may however vary between the samples. Assuming an ideal gas the air density varies with atmospheric conditions according to

$$\rho = p/(RT) \quad , \tag{2.4}$$

with

p	[Pa]	air pressure
R	[J /(kg K)]	specific gas constant, 287.05
T	[K]	temperature.

The samples are normalised according to the corresponding standard [2] by correcting the wind velocity using

$$U = U(\rho/\rho_0)^{\frac{1}{3}} \quad , \tag{2.5}$$

with

ρ_0	[kgm^{-3}]	reference air density, 1.225.

The density taken for calculation of Cp can then be taken constant as ρ_0.

Turbine 6

The data reduction procedure for turbine 6 is similar to the procedure for turbine 5. Differences from this procedure are itemized below. For more details on the data reduction procedure, please consult appendix B.2 which contains a summary of the results of this procedure.

Fatigue equivalent moments In addition to the same signals as for turbine 5, the fatigue equivalent flatwise and edgewise moments are acquired for two different material constants (steel and glass fibre). Rain flow counting was applied to the raw signal and the equivalent loads have readily been been determined in the database according to IEC 61400-13 [1].

Non-numeric values 'Not a number' values of the fatigue equivalent moments are excluded from the data set.

Controller update For turbine 6 the average calculated misalignment is not zero degree either. Potentially, controller updates by the manufacturer have resulted in numerous discontinuities of absolute nacelle direction over the measurement period. A data set is merged from samples between March 2005 to July 2007 and December 2007 to April 2009.

Wind direction Turbine 6 is positioned in the wake of turbine 5 for westerly wind directions which are therefore excluded. As for turbine 5, the disturbance directions due to the NM52 turbine south of the EWTW are also excluded. Since south easterly wind directions for turbine 6 are not obstructed by the meteorological mast, this sector is included as well. The resulting selected average wind directions are 110° to 140° and 200° to 250°.

Average pitch angle and variation The selection criteria are the same as for turbine 5, but the standard pitch angle for turbine 6 amounts to 0.1°.

Correction for atmospheric conditions Edgewise and flatwise moments scale differently with atmospheric conditions. The edgewise moment is dictated by gravity forces and the flatwise moment by aerodynamic force. The latter is influenced by atmosphere linearly through air density. The variation of the air density can be shown using equation 2.4 to lie between 1.18 and 1.28 kgm^{-3} for the selected samples. This is regarded as a small variation and hence the influence of atmospheric conditions is not taken into account, also not for the measured power of turbine 6.

2.2 Results

The number of remaining samples of the resulting data sets are summarized in Table 2.2. Figures illustrating the resulting data set are shown in appendix C. Figures C.1 and C.5 show the distribution of the samples as a function of wind speed and misalignment. Wind speeds around 8 m/s are most dominantly present. Also, the distribution of points is clearly not centered around a yaw angle of zero degrees. This is in agreement with the observations in section 2.1 (see also Figure 2.2a) and 2.1. For turbine 5, set 1 the samples are centered around approximately -12°, while for turbine 5, set 2 and turbine 6 this figure is -5°.

Table 2.2: Data set summary

Data set	pitch angle [°]	2 min average samples [-]	5 min average samples [-]	10 min average samples [-]
Turbine 5, set 1	0.065 $\pm$0.05	43165	13224	5193
Turbine 5, set 2	0.065 $\pm$0.05	22192	8084	2380
Turbine 6	0.100 $\pm$0.05	27328	9892	3682

Another interesting observation is that contrary to IEC 61400-1 3rd edition, the turbulence intensity increases with wind speed between 5 and 12 m/s (Figures C.4 and C.6). However Figure C.6d and C.6e indicate this to be a local increase since the turbulence intensity decreases again above 12 m/s. From previous measurements [16] it was illustrated that the variation of turbulence intensity influences the performance. This can partly be explained by the increase in available kinetic energy in the air, causing a higher effective local velocity. Also, an increased intensity enhances the flow mixture in the wake and hence the velocity deficit in the wake recovers faster. As a consequence the turbine power increases for an increasing turbulence intensity, next to the obvious increase of fatigue loads. It can be observed that although the intensity varies with wind speed roughly between 5% en 10%, the trend with yaw misalignment angle is more or less flat. Because of this flat trend and the fact that the effects of turbulence intensity on performance and loads are difficult to quantify, no correction is made for the influence of turbulence intensity.

Theoretically the turbines should operate at their optimal tip speed ratio (λ). In practice the rotational speed setting is limited by the converter, which means that the tip speed ratio (and thus the operating condition of the rotor) varies with wind speed even below rated conditions. This is illustrated in Figures C.3 and C.6. Therefore the results are presented not only as a function of yaw misalignment angle but also of wind speed bin. The influence of a varying tip speed ratio on the performance is expected to be dominant over the measured turbulence intensity variation. The results for power and loads dependence on yaw misalignment are given in the next sections.

Power

The results are presented in terms of Cp as defined in equation 2.3. As explained above the results for turbine 5 are normalised according to [2] whereas the results for turbine 6 are not. Generally speaking the qualitative trend between the three data sets is the same, as illustrated in Figures 2.3 and 2.4. The same holds for the difference between 2, 5 or 10 minute average samples, although the number of suitable samples for larger yaw angles is significantly less. Only negative yaw misalignment angles are registered here, but it should be noted that depending on the wind shear there can be significant differences in power between positive and negative angles.

Furthermore it can be observed that the trend of power coefficient with yaw misalignment angle varies with wind speed (or operational condition). The maximum power coefficient is reached close to or within the bin with the most samples. This indicates that the torque control of the turbine has been fine-tuned correctly to maximize yield.

More quantitative results in the form of line plots are shown in Figure 2.5. From Figure 2.5a it can be observed that also quantitatively the influence of averaging time is small. However the number of samples for large yaw misalignment is clearly smaller for an increasing averaging time and the standard error (indicated by the error bars) increases. Therefore 2 minute averages are taken for the following figures.

Figure 2.5b illustrates the differences between the three data sets. The fact that the power coefficients for turbine 6 are lower could be due to the fact that the pitch angle of this data set is higher. Also the

misalignment angle for the maximum power coefficient differs between the data sets. The value of ϕ_0 for curve fitting (equation 2.2) is taken as -2°, 0° and 0° for Turbine 5 (set 1), Turbine 5 (set 2) and Turbine 6 respectively. It is surprising that the maximum power coefficient does not appear for the misalignment angle that occurs most frequently.

Figure 2.5c and 2.5d show the influence of tip speed ratio on Cp. The resulting fitting parameters as outlined in section 2.1 are displayed in the legend. Both the absolute level and trend with yaw angle are clearly influenced by the tip speed ratio.

Figure 2.5e shows the resulting $Cp_0 - \lambda$ curve for all data sets and both 2 and 5 minute averages. The maximum power is attained around $\lambda = 8$ and Turbine 6 shows lower levels again. The power exponent β shows a clear increase with λ in Figure 2.5f. This implies a stronger dependency on yaw angle for an increased λ. For a small axial induction it seems logical that yawing the turbine does not greatly affect the turbine performance in comparison to a turbine operating at optimal axial induction ($a = 1/3$ at Cp_{max}). From the point of view of sectional airfoil aerodynamics, moving away from the angle of attack for maximum efficiency $(Cl/Cd)_{max}$ will lower the instantaneous power for both an increasing and decreasing angle of attack over a rotor revolution. Hence rotor averaged the power will decrease as well. For operation at a different angle of attack, this effect is probably less when averaged over a rotor revolution since the instantaneous power will increase or decrease depending on the sign of the angle of attack change. After the maximum power coefficient is obtained around $\lambda = 8$, the observed decrease of β is quite sudden. When the turbulent wake state is entered, the air behind the rotor 'stalls', i.e. the mass flux through the rotor becomes very low. Yawing of the turbine can have a favorable effect in this case since an extra mass flux is provided by the sideways flow. This in addition to the sectional airfoil aerodynamics probably explains why the exponent decreases more sudden for tip speed ratios above Cp_{max}.

Although the trends are clear, there is a significant amount of scatter between the data sets. The values of β roughly vary between 0.5 for a low tip speed ratio and 5 around maximum Cp. Previous research has reported similar values [6]. It seems rather obvious that the rotor operation condition (or rotor induction) influences how the turbine behaves in yawed flow. However the authors have not come across previous research on measurements that takes into account this dependency.

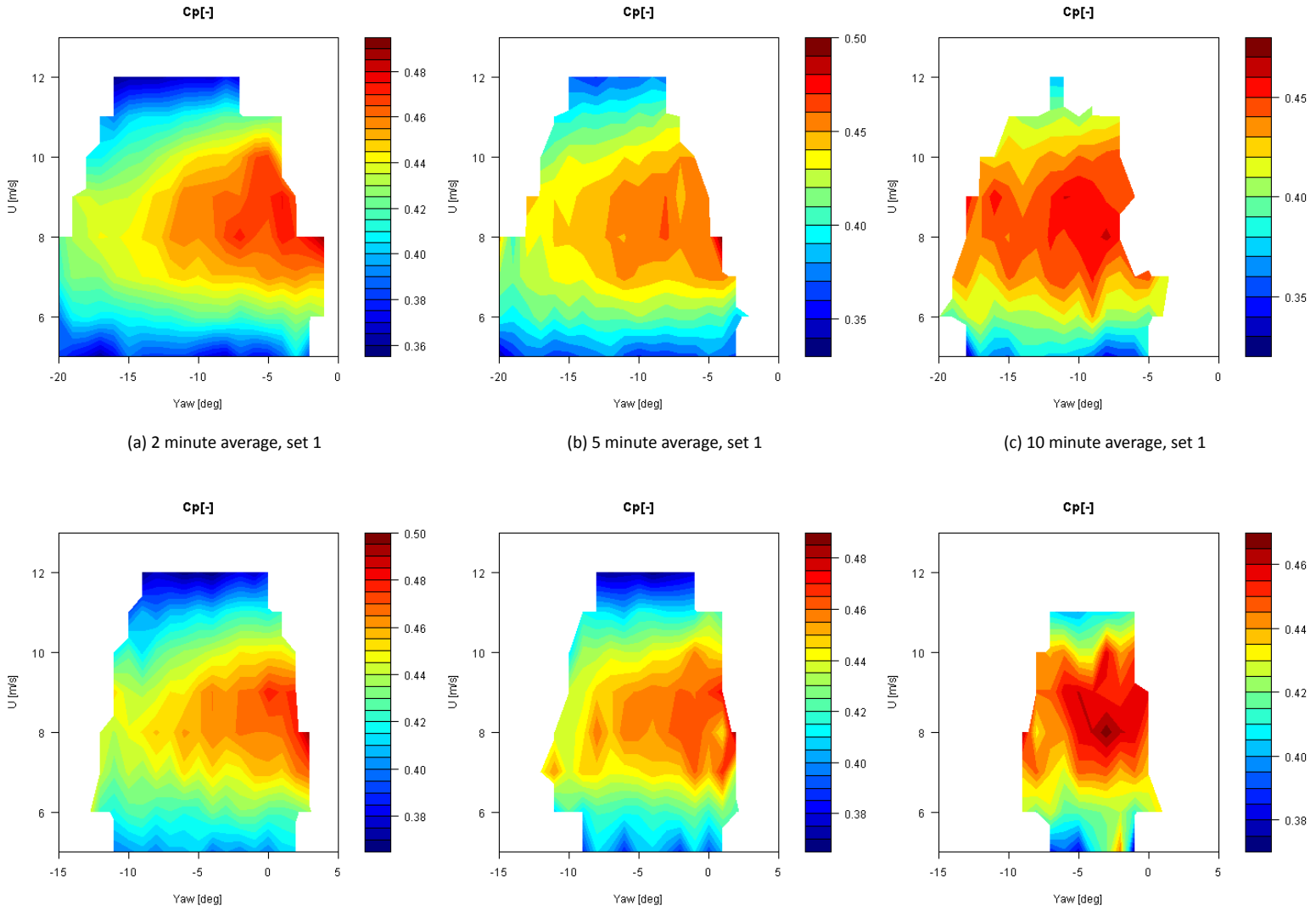

(a) 2 minute average, set 1

(b) 5 minute average, set 1

(c) 10 minute average, set 1

(d) 2 minute average, set 2

(e) 5 minute average, set 2

(f) 10 minute average, set 2

Figure 2.3: Power coefficient for data set 1 (above) and 2 (below), turbine 5

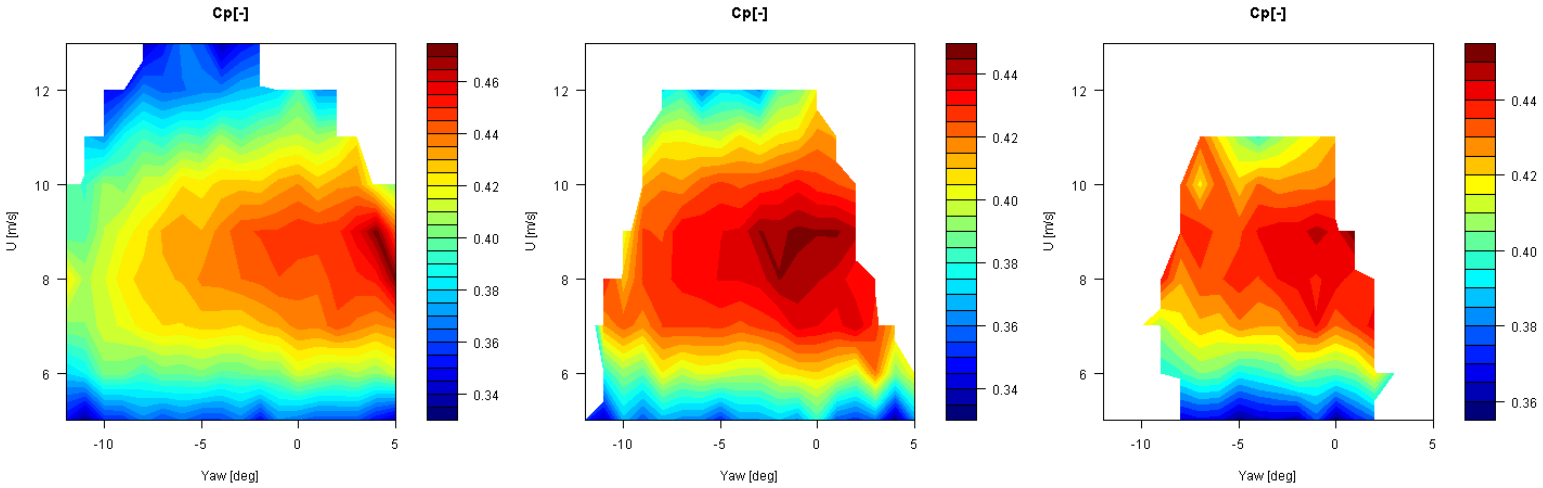

(a) 2 minute average

(b) 5 minute average

(c) 10 minute average

Figure 2.4: Power coefficient for turbine 6

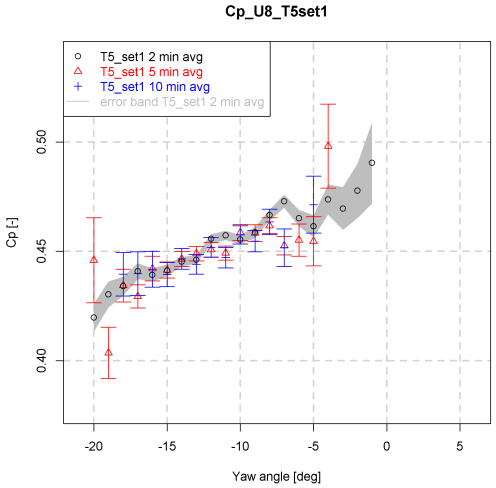

(a) Influence of averaging time (Turbine 5, set1, $U_{bin} = 8$ m/s)

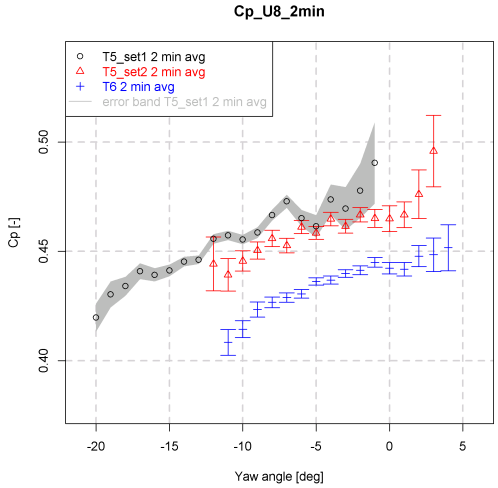

(b) Difference between data sets (2 min avg, $U_{bin} = 8$ m/s)

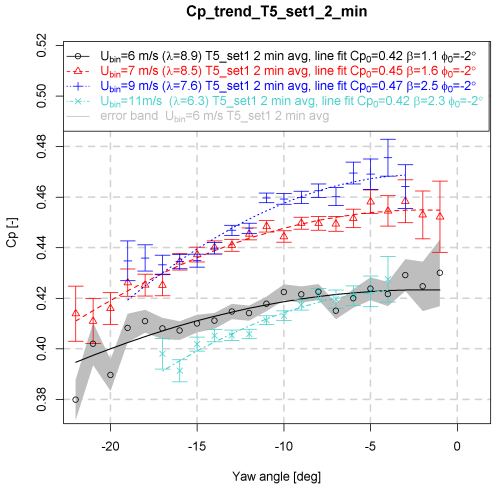

(c) Influence of tip speed ratio (Turbine 5, set1, 2 min avg)

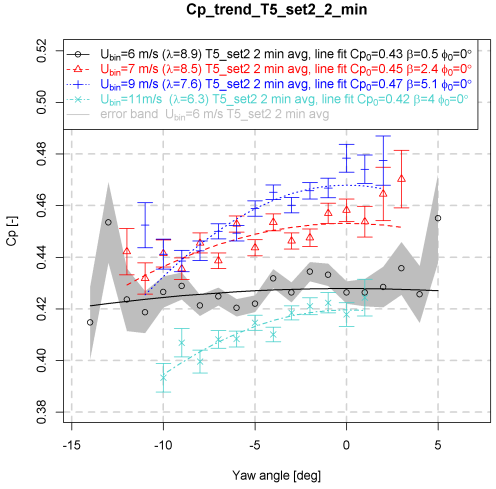

(d) Influence of tip speed ratio (Turbine 5, set2, 2 min avg)

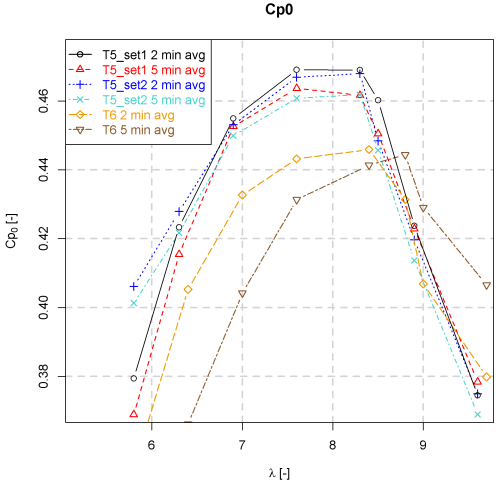

(e) Fitting parameter Cp_0 versus tip speed ratio λ

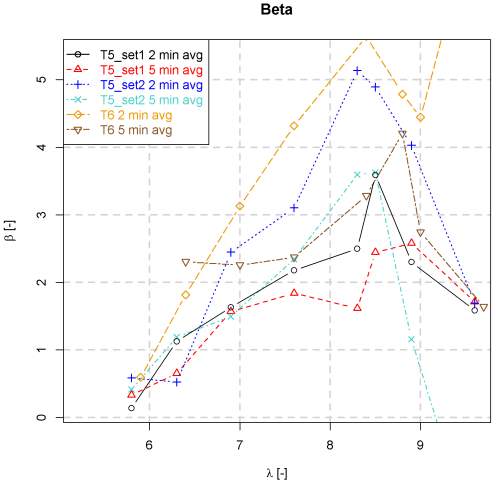

(f) Fitting parameter β versus tip speed ratio λ

Figure 2.5: Line plots of Cp and curve fitting parameters

Loads

Figure 2.6 show the edgewise fatigue equivalent loads for two different material constants. The edgewise loads are dominated by gravity forces and hence a variation with yaw angle is not present. A higher velocity indicates a higher rotational speed and hence more revolutions per average. This results in an increase of the fatigue equivalents edgewise loads.

Figure 2.7 show the flatwise fatigue equivalent loads for two different material constants. The flatwise moments are dominated by the unsteady wind loading. A higher velocity increases the number of cycles but a more dominant effect is the increased unsteady aerodynamic forces. Since turbine yaw misalignment influences these forces as well, a trend is expected with yaw angle.

A more quantitative comparison is shown in the line plots of Figure 2.8, displaying the data for the GFRP exponent. Figures 2.8a to 2.8d illustrate that also for the fatigue equivalent moments the difference between the three averaging periods is small. Therefore the 2 minute averages are judged to be representative. The trend of edgewise moment with yaw angle indeed is as good as flat (± 1% over 15° at U_{bin}=8 m/s). For the flatwise moment a trend is more clearly present as expected (± 20% decrease from -10° to 5° misalignment at U_{bin}=8 m/s). From the measured power values in section 2.2, one could tentatively conclude that the measured yaw angle for turbine 6 is calibrated correctly since $\phi_0 = 0$. The fact that the equivalent flatwise moment further decreases beyond zero degree yaw (hence no symmetry around zero degree yaw is observed) could well be attributed to the wind shear which counteracts the advancing and retreating blade effect for positive yaw.

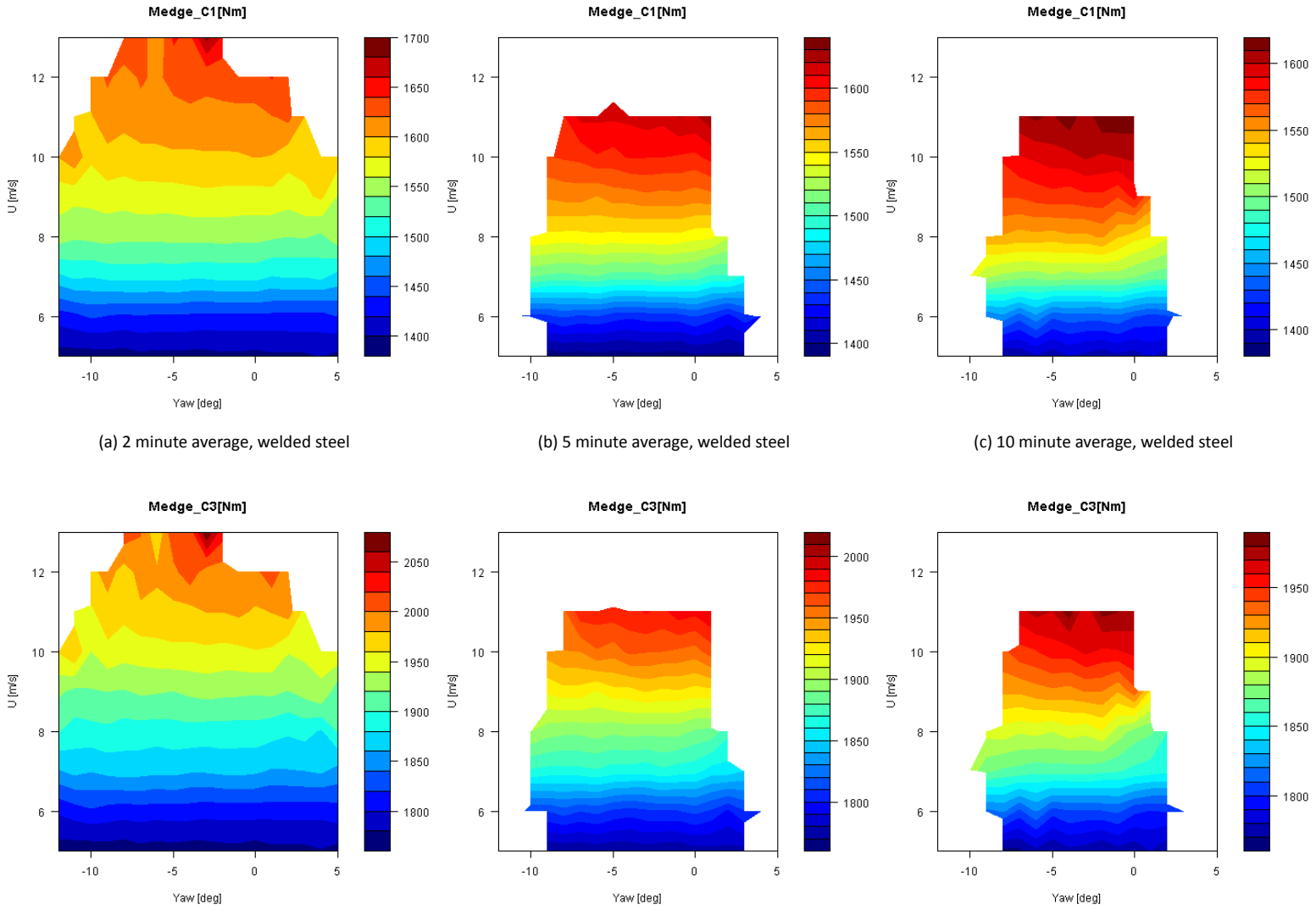

(a) 2 minute average, welded steel

(b) 5 minute average, welded steel

(c) 10 minute average, welded steel

(d) 2 minute average, GFRP

(e) 5 minute average, GFRP

(f) 10 minute average, GFRP

Figure 2.6: Fatigue equivalent blade root edgewise moment for welded steel (above) and GFRP (below), turbine 6

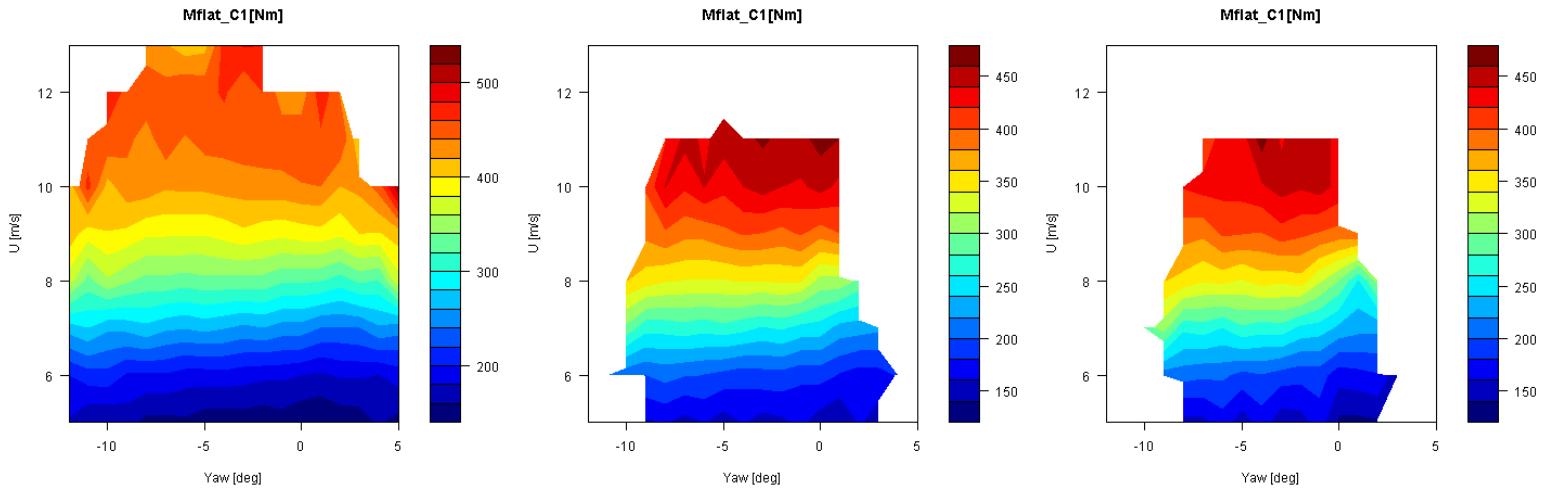

(a) 2 minute average, welded steel

(b) 5 minute average, welded steel

(c) 10 minute average, welded steel

(d) 2 minute average, GFRP

(e) 5 minute average, GFRP

(f) 10 minute average, GFRP

Figure 2.7: Fatigue equivalent blade root flatwise moment for welded steel (above) and GFRP (below), turbine 6

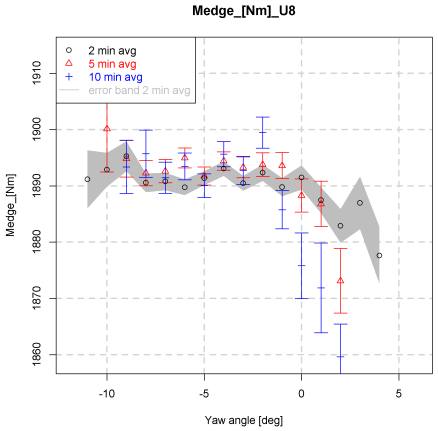

(a) Influence of averaging time on edgewise moment ($U_{bin} = 8$ m/s)

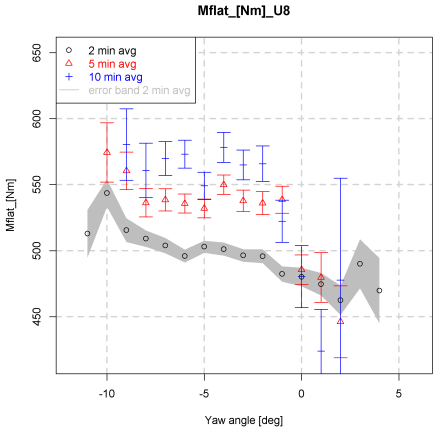

(b) Influence of averaging time on flatwise moment ($U_{bin} = 8$ m/s)

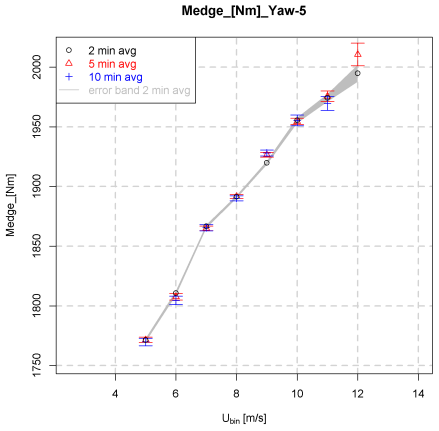

(c) Influence of wind speed on edgewise moment levels (Yaw=-5°)

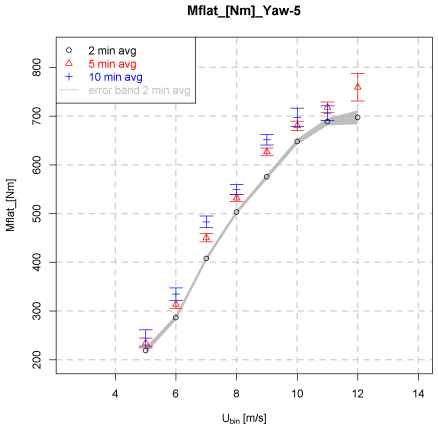

(d) Influence of wind speed on flatwise moment levels (Yaw=-5°)

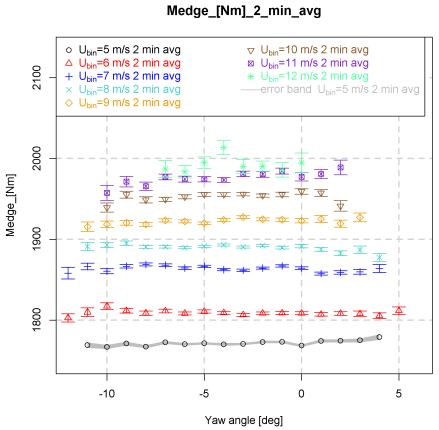

(e) Influence of wind speed on edgewise moment trend (2 min avg)

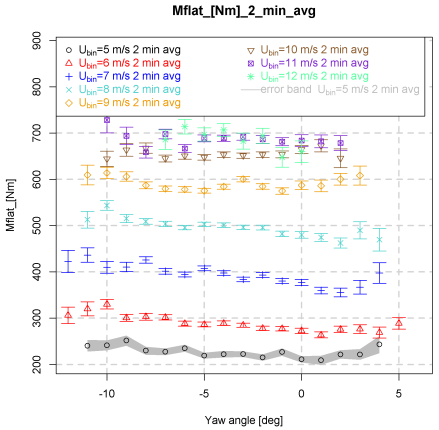

(f) Influence of wind speed on flatwise moment trend (2 min avg)

Figure 2.8: Line plots of fatigue equivalent moments for GFRP exponent

3
Computations

The effect of misalignment is studied numerically using a Blade Element Momentum (BEM) and a vortex line method. The results are compared to wind tunnel measurements and to the measured trends from section 2.2.

3.1 Model description

BEM modeling has been based on axial flow conditions and needs extensions to properly account for oblique inflow conditions. However this model is fast and is used widely throughout industry for certification purposes. A wide variation exist between implementations.

Vortex line models describe more of the flow physics and are therefore better suited for yawed flow predictions. Engineering extensions are not needed for oblique inflow as these effects are implicitly accounted for. The drawback lies in the increased computational effort associated with this method. Both models still need sectional aerodynamic coefficients as an input.

ECN has assembled the current state of the art of the above mentioned aerodynamic models in the `ECN Aero-Module` [4]. The included BEM model is based on the implementation in `PHATAS` [13], which has been refined through many years of usage in wind energy research and industry. Amongst the programmed extensions are the ECN dynamic inflow and the oblique inflow model.

The included vortex line method is the Aerodynamic Windturbine Simulation Module (`AWSM`) [27]. The `AWSM` code is based on generalized lifting line theory in combination with a free vortex wake method. The main assumption in this theory is that the extension of the geometry in spanwise direction is predominant compared to the ones in chord and thickness direction. Because of this, the real geometry is represented with a line passing through the quarter chord point of each cross section and all the flow field in chord-

wise direction is concentrated in that point. A complete description can be found in [27].

Oblique inflow modeling for BEM

The oblique inflow modeling for BEM applied in the ECN Aero-Module deserves special attention.

Momentum equations For oblique inflow, the axial momentum equation can be decomposed in rotor-axial and lateral direction. In the ECN Aero-Module, the sideways wind velocity is taken into account to determine equilibrium. Instead of solely solving the equation for the rotor-axial direction, the lateral momentum equation is included as well.

Skewed wake correction The oblique inflow results in an azimuthal variation of the wind velocity that is experienced by an element during a rotor revolution. This advancing and retreating blade effect is included by decomposing the wind and structural velocities in the right direction. To account for the variation of axial induction within each annulus due to the skewed wake, two models are implemented in the ECN Aero-Module. Both of these models relate the local axial induced velocity to the annulus averaged induced velocity through a skew factor.

- Glauert model
  The Glauert model [8] originates from helicopter theory and uses the wake skew angle rather than the rotor yaw angle to correct the induced velocities. The wake skew angle is defined as the angle of the actual flow leaving the turbine with the rotor axis. Using the rotor averaged induction the skew angle can be defined as [5]:
  $$\chi_s = \chi(1 + 0.6\overline{U_i}) \quad , \tag{3.1}$$
  with

χ_s	[rad]	wake skew angle
$\overline{U_i}$	[m/s]	rotor averaged axial induced velocity.

  The local induced velocity U_i is then related to the annulus averaged velocity using
  $$U_i = U_{i,ann}(1 + \frac{15\pi}{32}\frac{r}{R}\tan\frac{\chi}{2}\cos\phi) \quad , \tag{3.2}$$
  with

$U_{i,ann}$	[m/s]	annulus averaged axial induction
$\frac{r}{R}$	[-]	ratio of local radius and tip radius measured in rotorplane
ϕ	[rad]	azimuth angle (zero at most downwind position).

- Schepers model
  The model as defined by Schepers [19, 22] and implemented in PHATAS [13] has purposely been developed for wind turbines. Similar to the Glauert model, a skew function is determined for each element as a function of effective yaw angle, azimuth angle and radial location. This skew function

then relates the local induction at each element to the annulus averaged axial induction. This skew function was originally developed from the correlation between annulus averaged and local induction velocities for an annulus by means of wind tunnel measurements. The main difference in comparison to the Glauert model lies in the refinement between inboard and outboard sections through inclusion of the effects of the root vortex.

Dynamic stall modeling The blade section of a wind turbine in yaw experiences a continuously changing angle of attack. Especially for the inboard sections this implies dynamic stall effects to occur and influence the blade loading. Two different models are implemented in the `ECN Aero-Module` to account for these effects.

- Snel model
  This models account for dynamic effects in separated flow and is especially developed for application in a wind turbine environment. Its numerical implementation does not require inputting airfoil specific parameters, which makes it popular for application in an aero-elastic code. The first order model consists of a linear differential equation for the dynamic lift increment, driven by the difference with the potential flow lift and angle of attack history. The second order model includes the first order model and adds higher frequency dynamics of self excited nature. More details can be found in [26].

- Beddoes-Leishman model
  The emphasis of the Beddoes-Leishman method lies on a more complete physical representation of the overall unsteady aerodynamics. Although originating from helicopter research, it is intended as a general model for airfoils undergoing dynamic stall. The model essentially consists of four subsystems:

  1. Attached flow model, including an impulsive component and circulatory (shed vorticity) component.
  2. A trailing edge separation module to include the effect of the dynamic separation point position.
  3. A leading edge separation module to predict dynamic stall onset. Leading edge separation lag is included.
  4. A vortex module to calculate the possible vortex induced aerodynamic forces.

  These four sub-models are connected in an open loop system, where output from one model serves as input for the next. More details can be found in [11, 12]. The specific implementation in the `ECN Aero-Module` is based on the work described in [3], [9] and [18]. Further details concerning its implementation are given in appendix D.

3.2 Settings

Calculations have been performed for a rigid model with a constant wind (no turbulence). The MEXICO [23] and Nasa-Ames [25] model have been taken as subject of investigation since these models are extensively documented and a wide variety of measured results are available.

To investigate the influence of wind shear on the loads, calculations have been performed with and without wind shear. Since the MEXICO and Nasa-Ames rotor feature a much lower hub height than 'real-life' turbines, an equivalent wind shear has been used by applying a roughness length of 0.0025 m and 0.006 m respectively. To cover the operational range , three tip speed ratios are included (U_∞=10, 15 and 24 m/s) for the MEXICO simulations. These three cases represent turbulent wake state, design conditions and separated flow conditions respectively. The Nasa-Ames measurements mostly represent low tip speed ratios and stalled airfoil conditions.

The AWSM calculations have been performed without dynamic stall model. Yaw angles were simulated between 0° and 30° yaw in steps of 2.5° or 5°. BEM calculations have been performed between -30° and 30° yaw. It should be noted that this range is considerably larger than obtained from the field measurements. A time step corresponding to a step in azimuth of 10° has been applied. The BEM calculations feature both the Glauert and Schepers model for yaw as well the Snel and Beddoes Leishman model for dynamic stall.

3.3 Results

The results are presented for both power and axial force as well as for the fatigue loads. The legend indication is further clarified in Table 3.1. To facilitate focusing on the trend with yaw misalignment angle, the power and axial force results are divided by the corresponding value at zero yaw (i.e. Cp/Cp_0 and $Cdax/Cdax_0$). The computed absolute value results are compared in section E to check that the flow physics are well approximated for axial inflow conditions.

Table 3.1: Legend clarification for calculations

	Yaw model	Dynamic stall model
BEM	Schepers	Snel
BEM-Beddoes	Schepers	Beddoes Leishman
BEM-Glauert	Glauert	Snel
BEM-Glauert-Beddoes	Glauert	Beddoes Leishman

Power and axial force

The presented power and axial force values are a result of averaging these over a rotor revolution. Although the computations have also been performed with wind shear included, these results have been omitted here since its influence on the averaged power and axial force was almost negligible. This also holds for the time averaged differences between positive and negative yaw misalignment.

In a more extreme wind shear however this effect is expected to become more significant. Figures 3.1a to 3.1c display the power coefficient divided by its maximum value (Cp/Cp_0) to reveal the trend with yaw angle for the MEXICO results. As expected, the influence of yaw and dynamic stall model is negligible for the time averaged quantities. Apart from the turbulent wake state, the trend between BEM and AWSM is very similar. The increase in power for a misaligned turbine as predicted by BEM in Figure 3.1a is a result of the formulation of the momentum equations as discussed in section 3.1. As was explained for the field measurements (section 2.2), yawing the turbine reduces the amount of 'stalled flow' (a reduced mass flux) behind the rotor for the turbulent wake state. Apparently this effect is estimated to be less strong for AWSM.

Figures 3.2a to 3.2c display the power coefficient for the Nasa-Ames results including the measured trend by a torque sensor. The Nasa-Ames measurements for U_∞ =10 m/s and U_∞ =15 m/s feature stalled conditions, with an angle of attack around $\alpha \approx 14^\circ$ and $\alpha \approx 23^\circ$ respectively in the outboard sections. It is surprising to see the power increase with yaw angle for these conditions. Possibly the advancing and retreating blade effect results in (more) attached flow conditions in the advancing half of the rotor plane, thereby increasing the rotor averaged torque. The same trend has been presented in [24], which also includes a more detailed view on the corresponding sectional flow physics. Dynamic stall modeling becomes important for these conditions, which can explain why BEM is in better agreement with the measurements than AWSM (the AWSM calculations do not include a dynamic stall model). Also a difference between the Snel en Beddoes Leishman model can be observed.

The resulting exponents β of equation 2.2 are given in Table 3.2. The values are much smaller than

Table 3.2: Summary of resulting curve fitting parameter β values

Data set	U_∞ [m/s]	λ [-]	a[-]†	β[-]		
				BEM	AWSM	measured
MEXICO	10	10.0	0.41	-0.09	1.44	NA
MEXICO	15	6.7	0.26	1.30	1.68	NA
MEXICO	24	4.2	0.11	0.66	0.74	NA
Nasa-Ames	5	7.5	0.21	1.49	2.00	2.13
Nasa-Ames	10	3.8	0.08	0.40	0.83	-0.19
Nasa-Ames	15	2.5	0.03	-2.95	-0.76	-2.76

† Rotor averaged axial induction factor (approximate)

the values deduced from the field measurements in Figure 2.5f. Here it must be noted that the range of measured yaw angles in section 2.2 is much smaller compared to the calculations, which are

performed between -30° and 30°. In addition to that the field measurements are not corrected for variations in turbulence intensity. Since a clear variation of turbulence intensity with wind speed is present (Figure C.4), this effect can influence the measured trend of β as a function of wind speed. However, the trend of an increasing exponent towards maximum Cp and a decrease for the turbulent wake state for all calculations and measurements is the same as for the field measurements. At design conditions, the low value of β from BEM in comparison to the measurements is consistent with previous observations [20].

Figures 3.1d to 3.1f and 3.2d to 3.2f display the axial force coefficient divided by its maximum value ($Cdax/Cdax_0$) to reveal the trend with yaw angle. A trend similar to the results for the power coefficient is obtained. The discussed trend for the turbulent wake state (Figure 3.1d)seems to be predicted well by AWSM in comparison to the measurements. This seems to indicate that there is room for improvement in the momentum equations as used in the BEM model. For design conditions (Figure 3.1e), a good agreement is shown for both BEM and AWSM compared to the measured values. For low induction at separated flow conditions (Figures 3.1f,3.2e and 3.2f), both calculation methods under predict the trend with yaw angle. Both models feature a sectional approach based on the input of airfoil data, which is difficult to justify for separated flow conditions because of its inherently three-dimensional character. In addition to that, sectional characteristics for high angles of attack are often not measured and therefore based on an inaccurate estimate.

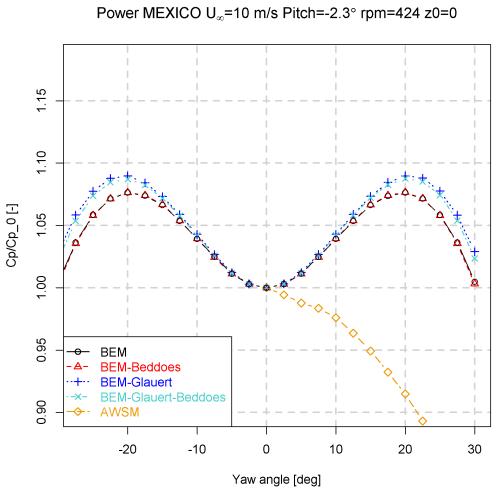

(a) Cp/Cp_0, $U_\infty = 10$ m/s, $\lambda = 10.0$

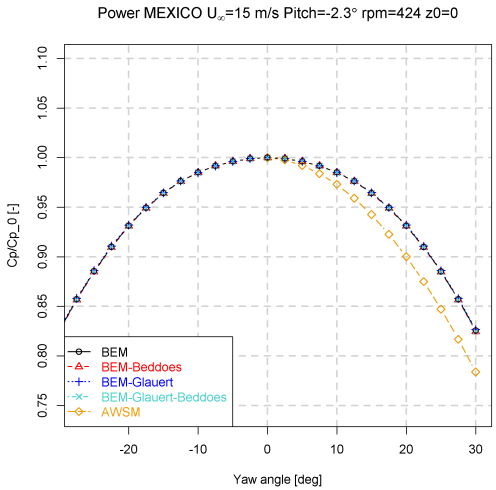

(b) Cp/Cp_0, $U_\infty = 15$ m/s, $\lambda = 6.7$

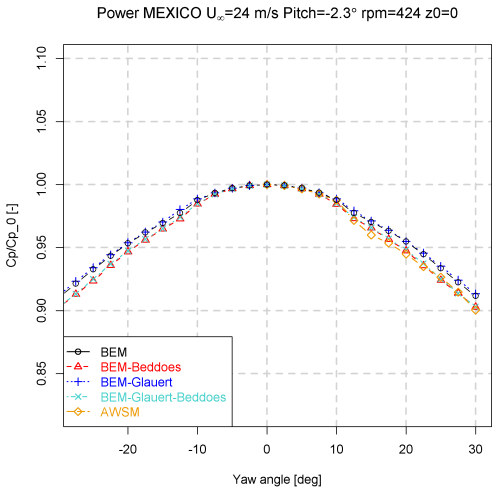

(c) Cp/Cp_0, $U_\infty = 24$ m/s, $\lambda = 4.2$

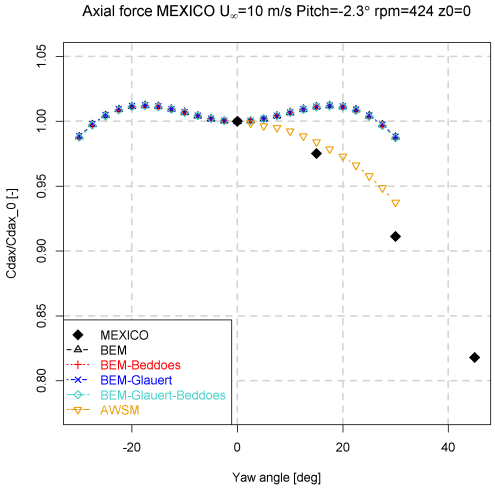

(d) $Cdax/Cdax_0$, $U_\infty = 10$ m/s, $\lambda = 10.0$

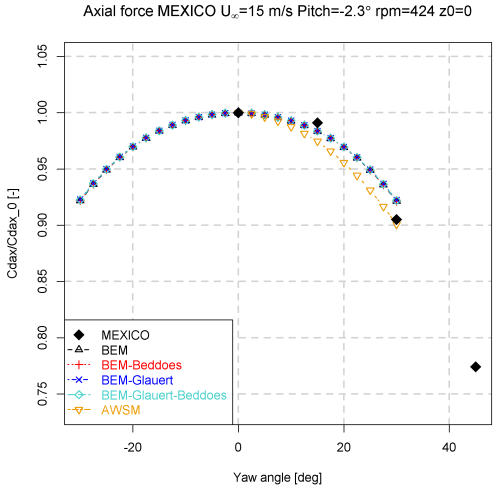

(e) $Cdax/Cdax_0$, $U_\infty = 15$ m/s, $\lambda = 6.7$

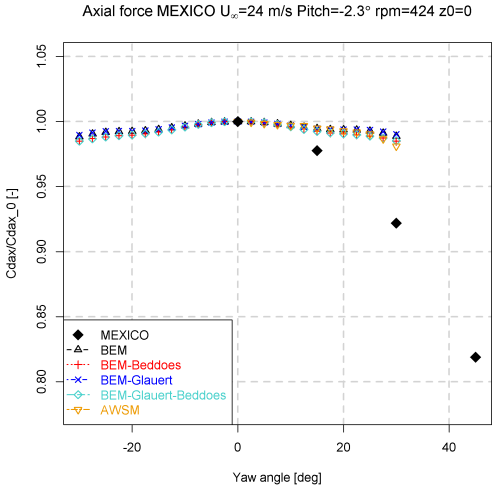

(f) $Cdax/Cdax_0$, $U_\infty = 24$ m/s, $\lambda = 4.2$

Figure 3.1: MEXICO power coefficient (above) and axial force coefficient trend (below) for different operating conditions

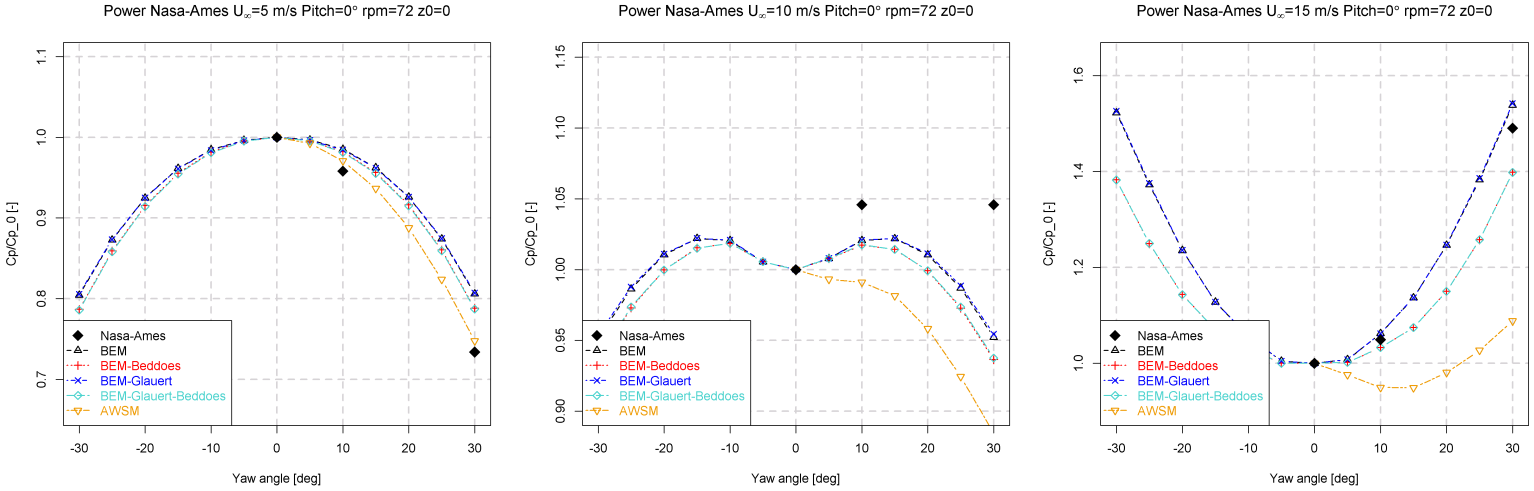

(a) Cp/Cp_0, $U_\infty = 5$ m/s, $\lambda = 7.5$ (b) Cp/Cp_0, $U_\infty = 10$ m/s, $\lambda = 3.8$ (c) Cp/Cp_0, $U_\infty = 15$ m/s, $\lambda = 2.5$

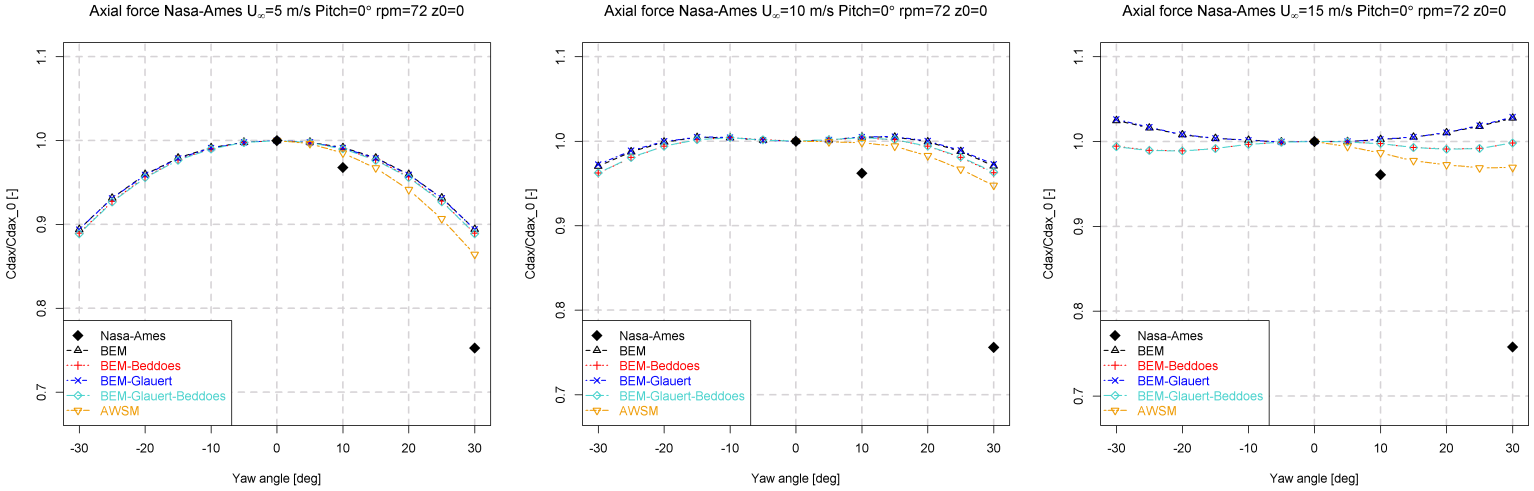

(d) $Cdax/Cdax_0$, $U_\infty = 5$ m/s, $\lambda = 7.5$ (e) $Cdax/Cdax_0$, $U_\infty = 10$ m/s, $\lambda = 3.8$ (f) $Cdax/Cdax_0$, $U_\infty = 15$ m/s, $\lambda = 2.5$

Figure 3.2: Nasa-Ames power coefficient (above) and axial force coefficient trend (below) for different operating conditions

Loads

Finally the loads are compared. The flapwise fatigue equivalent moment is obtained by analyzing the time series of the flapwise moment. A similar routine is used compared to the post-processing of the field measurements. The results are shown in Figure 3.3 for MEXICO calculations with and without wind shear and Figure 3.4 for Nasa-Ames calculations without shear. It is clearly illustrated that the wind shear removes the symmetry around zero degree yaw. As explained in section 2.2 this is because the wind shear counteracts the advancing and retreating blade effect for positive yaw.

Opposite to the field measurements, a clear trend is observed with yaw angle for the calculations. Here it must be noted again that the calculations feature a much wider range of yaw angles. In addition to that it is expected that the influence of blade flexibility and turbulence (which are not taken into account here) will further flatten the observed trend.

In agreement with expectations, the influence of the chosen yaw model for BEM is larger for a higher rotor induction. The Schepers model predicts lower values than the Glauert model, and is in better agreement with AWSM. Differences up to 50% are shown at U_∞=10 m/s, Yaw=30°. Apart from the offset, the measured MEXICO strange gauge data shows a similar trend to the Schepers model. The Beddoes Leishman model generally predicts slightly lower fatigue moments than the Snel model. To illustrate the cause for these differences, the sectional normal forces are plotted as a function of azimuth angle in Figure 3.5. Although the results are in good agreement for the outboard sections, the inboard sections clearly show a different trend with azimuth angle for the various models. The measured data as well as the AWSM and BEM Schepers simulation feature a normal force peak in the upwind half of the rotorplane, whilst the BEM Glauert model predicts this peak to occur in the downstream half. The fact that the inboard and outboard contribution appear to be out of phase can explain why the total flapwise fatigue equivalent moments are lower for the Schepers model.

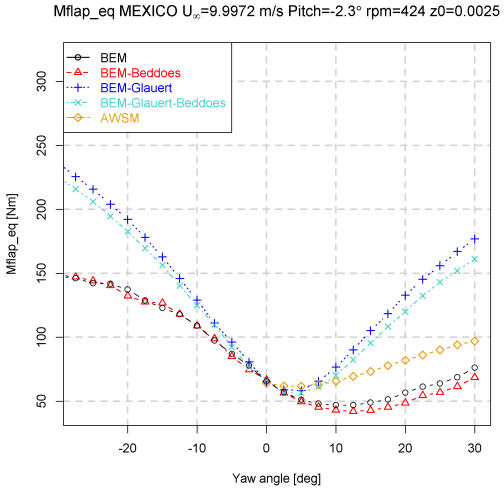

(a) $U_\infty = 10$ m/s, $\lambda = 10.0$, windshear

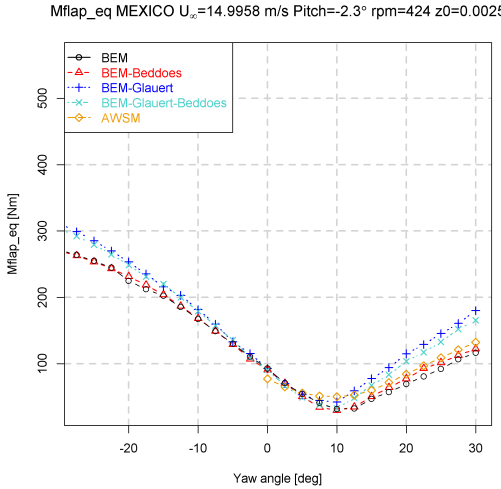

(b) $U_\infty = 15$ m/s, $\lambda = 6.7$, windshear

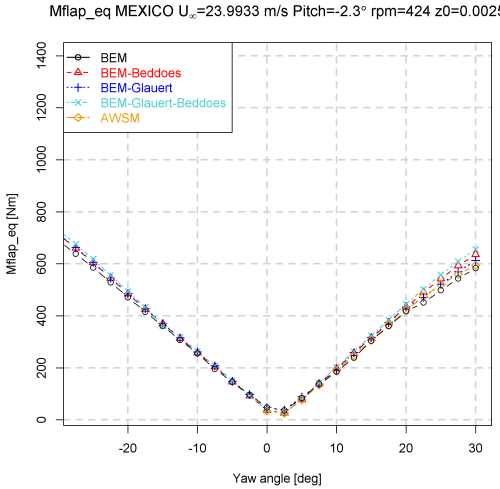

(c) $U_\infty = 24$ m/s, $\lambda = 4.2$, windshear

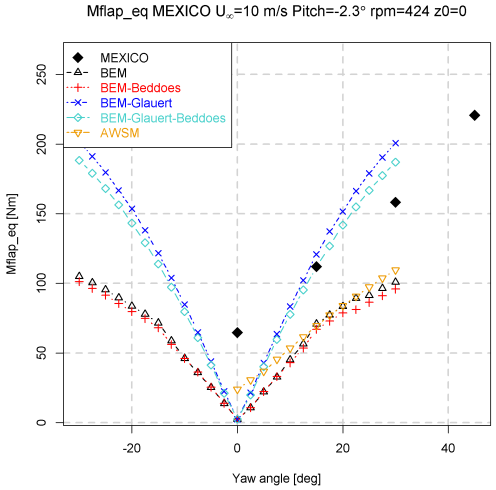

(d) $U_\infty = 10$ m/s, $\lambda = 10.0$, no windshear

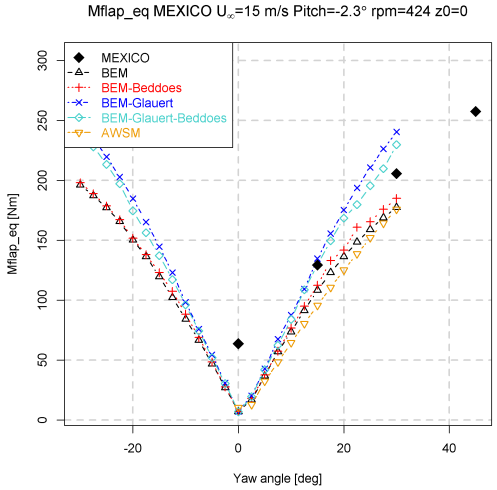

(e) $U_\infty = 15$ m/s, $\lambda = 6.7$, no windshear

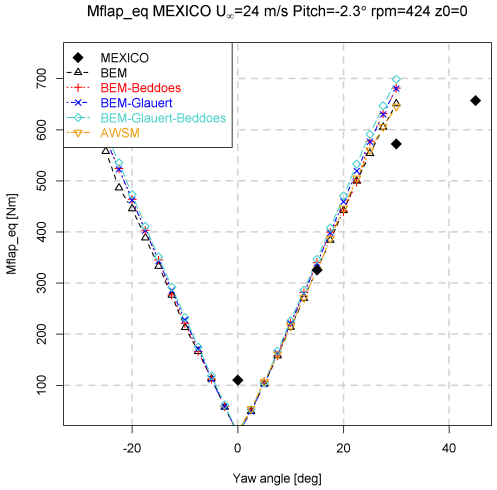

(f) $U_\infty = 24$ m/s, $\lambda = 4.2$, no windshear

Figure 3.3: MEXICO flapwise fatigue equivalent blade root bending moment with windshear (above) and and without windshear (below) for different operating conditions

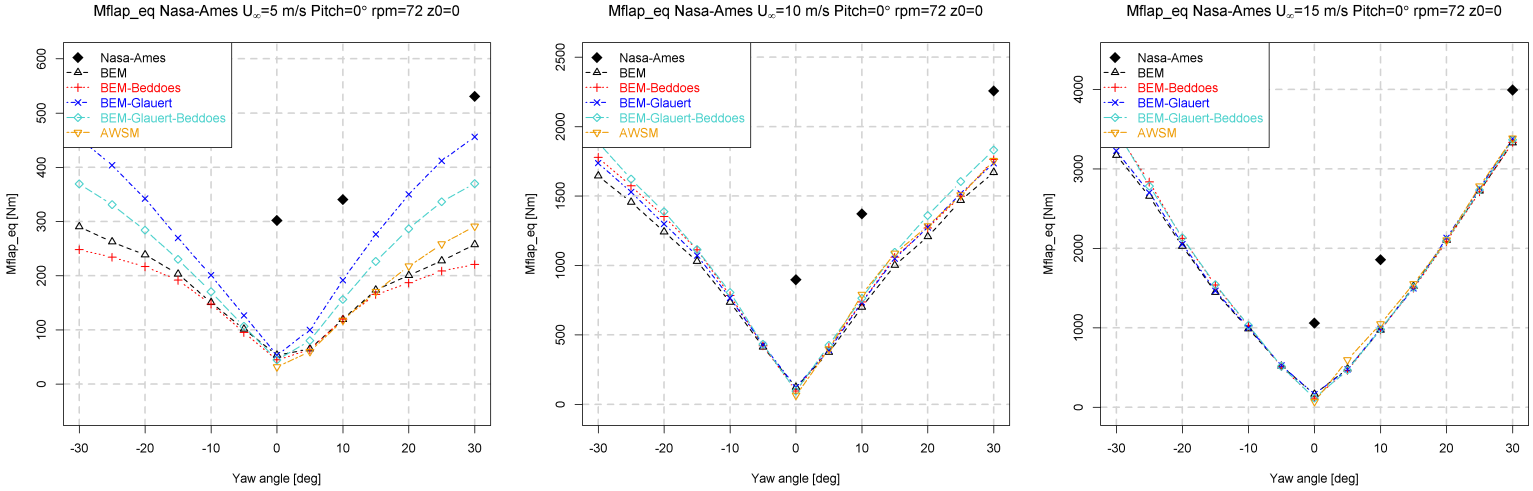

(a) $U_\infty = 5$ m/s, $\lambda = 7.5$, no windshear (b) $U_\infty = 10$ m/s, $\lambda = 3.8$, no windshear (c) $U_\infty = 15$ m/s, $\lambda = 2.5$, no windshear

Figure 3.4: Nasa-Ames flapwise fatigue equivalent blade root bending moment without windshear for different operating conditions

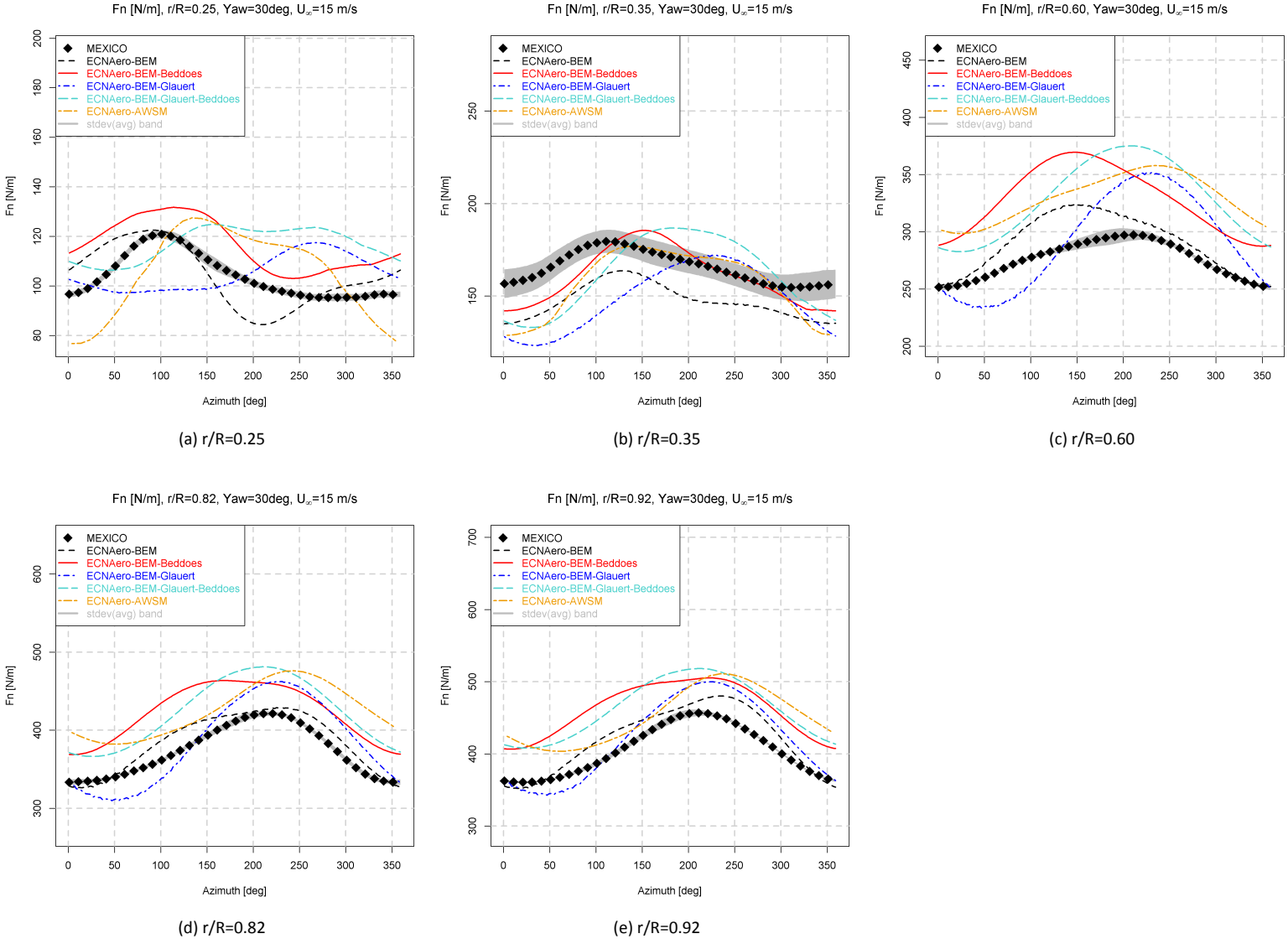

(a) r/R=0.25 (b) r/R=0.35 (c) r/R=0.60

(d) r/R=0.82 (e) r/R=0.92

Figure 3.5: MEXICO normal force variation (perpendicular to the local chord) as a function of azimuth angle, U_∞=15 m/s, Yaw=30°, no windshear

4

Conclusions and recommendations

The effect of yaw misalignment on performance and loads of a single wind turbine is investigated using both field and wind tunnel measurements and simulations.

The power trend with yaw is shown to strongly depend on the operational condition. From low rotor induction up to the turbulent wake state the power exponent for cosine fitting is shown to increase. From the turbulent wake state onwards this exponent is shown to decrease again. The difference in absolute values of this factor between field measurements and computations is mainly attributed to the limited yaw angle range available of the field measurement data. Discrepancies between the different calculation models indicate there is room for improvement of the BEM momentum equations for oblique inflow. For deeply separated flow conditions, the power is even shown to increase with yaw angle. In these cases dynamic stall modeling becomes important also for the prediction of the rotor averaged torque.

The trend of fatigue equivalent edgewise moments with misalignment is flat as expected due to the dominant contribution of gravitational loads. The measured flatwise moments feature more of a trend and appear to be distributed asymmetric around zero degree yaw. This is caused by the wind shear counteracting the advancing and retreating blade effect for positive misalignment.

The modeling of the skewed wake effect for BEM significantly influences the predicted fatigue equivalent flatwise moments for design conditions. The fact that the inboard and outboard contribution appear to be out of phase can explain why the total flapwise fatigue equivalent moments are lower for the Schepers model compared to the Glauert model. The good agreement with AWSM predictions and the measured MEXICO trend are in favor of applying the Schepers model for BEM calculations. The load discrepancies for the different applied dynamic stall models are small, except for separated flow conditions at very low tip speed ratios.

To reduce the standard error of the field data it is recommended to obtain more measurements. It would be helpful if the different data sets due to resetting the turbine signals (nacelle direction) can be merged. To increase the available data for larger yaw angles, it would be beneficial if the wind turbines can be operated at a constant yaw for a limited time period. In addition to that it is recommended to correct the field measured performance for turbulence intensity variations to enable a more accurate prediction of the power exponent β as a function of wind speed.

For the calculations it is recommended to include the effects of turbulence and flexibility (especially for the loads). Simulating the turbines used in the field in addition to the MEXICO and Nasa-Ames turbine should allow a more direct comparison with the field measurements.

Bibliography

1 IEC TS 61400-13, Wind turbine generator systems Part 13: Measurement of mechanical loads, June 2001.

2 IEC TS 61400-12-1, Wind turbines Part 12-1: Power performance measurements of electricity producing wind turbines, 2005.

3 A. Björck. DYNSTALL: Subroutine package with a dynamic stall model. Technical Report FFAP-V-110, FFA, Sweden, 2000.

4 K. Boorsma, F. Grasso, and J.G. Holierhoek. Enhanced approach for simulation of rotor aerodynamic loads. Technical Report ECN-M–12-003, ECN, presented at EWEA Offshore 2011, Amsterdam, 29 November 2011 - 1 December 2011, 2011.

5 T. Burton, D. Sharpe, N. Jenkins, and E. Bossanyi. *Wind Energy Handbook*. John Wiley & Sons, Ltd., 2001.

6 Jan-Åke Dahlberg and Björn Montgomerie. Research Program of the Utgrunden Demonstration Offshore Wind Farm, Final Report: Part II Wake Effects and Other Loads. Technical report, FOI Department of Wind Energy Research, 2005.

7 P.J. Eecen et al. Measurements at the ECN wind turbine test station wieringermeer. Technical Report ECN-RX–06-055, ECN, 2006.

8 H. Glauert. A General Theory of the Autogyro. Technical Report ARC R&M No.1111, ARC R&M, 1926.

9 J.G. Holierhoek, J.B. De Vaal, A. H. Van Zuijlen, and H. Bijl. Comparing different dynamic stall models. *Wind Energy*, online 2012, 2012.

10 F.A. Kaandorp. Private communication, July 2012.

11 J.G. Leishman and T.K. Beddoes. A generalized method for unsteady airfol behaviour and dynamic stall using the indicial method. In *42nd Annual Forum*, Washington D.C., June 1986. American Helicopter Society.

12 J.G. Leishman and T.K. Beddoes. A semi-empirical model for dynamic stall. *Journal of the American Helicopter Society*, 34:3–17, 1989.

13 C. Lindenburg and J.G. Schepers. Phatas-iv aeroelastic modelling, release ”dec-1999” and ”nov-2000”. Technical Report ECN-CX–00-027, ECN, 2000.

14 L.A.H. Machielse. Fatigue equivalent blade root moments in a misaligned 2.5 MW turbine. Technical Report ECN-Wind Memo-12-013, ECN, 2012.

15 L.A.H. Machielse. Performance coefficients in a misaligned 2.5 MW turbine. Technical Report ECN-Wind Memo-12-012, ECN, 2012.

16 Machielse, L.A.H. Validatiemetingen EWTW, Eindrapport. Technical Report ECN-E–06-062, ECN, 2006.

17 T.S. Obdam. Validation of wind farm production calculations by WAsP and FarmFlow using EWTW measurements. Technical Report ECN Wind Memo-06-090, ECN, 2006.

18 R. Santos Pereira, J.G. Schepers and M. Pavel. “Validation of the Beddoes Leishman Dynamic Stall model for Horizontal Axis Wind Turbines using Mexico data”. In *49th AIAA Aerospace Sciences meeting*, January 2011.

19 J.G. Schepers. An engineering model for yawed conditions, developed on basis of wind tunnel measurements. Technical Report AIAA-1999-0039, AIAA, 1999.

20 J.G. Schepers. *Engineering models in wind energy aerodynamics. Development, implementation and analysis using dedicated aerodynamic measurements*. PhD thesis, Delft University of Technology, November 2012.

21 J.G. Schepers, K. Boorsma, et al. Final report of IEA Task 29, Mexnext (Phase 1), Analysis of Mexico wind tunnel measurements. Technical Report ECN-E-12-004, Energy research Center of the Netherlands, ECN, December 2011.

22 J.G. Schepers and Vermeer L.J. Een engineering model voor scheefstand op basis van windtunnelmetingen. Technical Report ECN-CX–98-070, ECN, 1998.

23 J.G. Schepers and H. Snel. Model Experiments in Controlled Conditions, Final report. Technical Report ECN-E–07-042, ECN, 2007.

24 S.J Schreck and J.G. Schepers. Unconventional Rotor Power Response to Yaw Error Variations. In *Annual IEA Task 29 meeting, NREL, NWTC, Boulder, CO USA*, November 2012.

25 D. Simms, M. Hand, L.J. Fingersh, and D. Jager. Unsteady Aerodynamics Experiment Phases II-IV Test Configurations and Available Data Campaigns. Technical Report NREL/TP-500-25950, NREL, 1999.

26 H. Snel. Heuristic modelling of dynamic stall characteristics. In *Conference proceedings European Wind Energy Conference*, pages 429–433, Dublin, Ireland, October 1997.

27 A. Van Garrel. Development of a wind turbine aerodynamics simulation module. Technical Report ECN-C–03-079, ECN, 2003.

A

SQL scripts

A.1 Turbine 5

SQL script for turbine 5 power (2 minute average)

```
select
"t_0",
"MM3_WS80_240_2min_avg","MM3_WS80_240_2min_std",
"MM3_WD80_240_2min_avg","MM3_WD80_240_2min_std",
"MM3_Pair80_2min_avg",
"MM3_Tair80_2min_avg",
"T5_Pwsnac_2min_avg",

"T5_PEpow_2min_avg",
"T5_Pnacdrtn_2min_avg","T5_Pnacdrtn_2min_std",
"T5_Popmode_2min_min","T5_Popmode_2min_max",
"T5_Ppitch1_2min_min","T5_Ppitch1_2min_max",
"T5_Rspd_2min_avg","T5_Rspd_2min_std",
"MM3_WS80_true_2min_avg",
"MM3_WS80_true_2min_std",
"MM3_WS52_true_2min_avg"

from public."statistics_2m"

where "MM3_WD80_240_2min_avg">135 and "MM3_WD80_240_2min_avg"<300 and
"T5_Popmode_2min_max"<14.5 and "T5_Popmode_2min_min">11 and
```

```
"T5_PEpow_2min_avg">25
```

A.2 Turbine 6

SQL script for turbine 6 loads (2 minute average)

```
select * from
(
select
"t_0",
"MM3_WS80_240_2min_avg","MM3_WS80_240_2min_std",
"MM3_WD80_240_2min_avg","MM3_WD80_240_2min_std",
"MM3_Pair80_2min_avg",
"MM3_Tair80_2min_avg",
"T6_Pwsnac_2min_avg",

"T6_PEpow_2min_avg",
"T6_Pnacdrtn_2min_avg","T6_Pnacdrtn_2min_std",
"T6_Popmode_2min_min","T6_Popmode_2min_max",
"T6_Ppitch1_2min_min","T6_Ppitch1_2min_max",
"T6_Rspd_2min_avg","T6_Rspd_2min_std",
"MM3_WS80_true_2min_avg",
"MM3_WS80_true_2min_std",
"MM3_WS52_true_2min_avg"

from public."statistics_2m"

where
"MM3_WD80_240_2min_avg">110 and "MM3_WD80_240_2min_avg"<140 or
"MM3_WD80_240_2min_avg">200 and "MM3_WD80_240_2min_avg"<250 and
"T6_Popmode_2min_min">10.8 and "T6_Popmode_2min_min"<11.2 and
"T6_PEpow_2min_avg">25 and "T6_Pnacdrtn_2min_std"<1
) as "r1" join
(
select
  "t_0",
  "T6_Mbe1_load_P_2min_eql_C1", "T6_Mbe1_load_P_2min_eql_C3",
  "T6_Mbf1_load_P_2min_eql_C1", "T6_Mbf1_load_P_2min_eql_C3"
from public.eql_2m
```

```
) as "r2"
on (r1.t_0 = r2.t_0)
order by r1."t_0"
```

B

Data reduction logs

B.1 Turbine 5

Data reduction log for turbine 5 power dataset 1 (2 minute average)

```
"start length:770909"
"NaN in yaw:11330"
"data set 1 :458578"
"NA in Pair:0"
"wind dir (220 to 280deg) :160554"
"power>25:0"
"op_mode (11 to 11.2) :29638"
"nacelle dir std (<1) :20637"
"windspeed (5 to 13 m/s) :11718"
"v/v_nac (0.9 to 1.1) :18376"
"TI (0.01 to 0.2) :871"
"pitch_dif (<0.05 deg) :2143"
"wind shear ws80/ws50 (1 to 1.2 ):11319"
"pitch_angle (0.065 deg) :2580"
"final length:43165"
```

Data reduction log for turbine 5 power dataset 1 (5 minute average)

"start length:296096"
"NaN in yaw:4551"
"data set 1 :186544"
"NA in Pair:0"
"wind dir (220 to 280deg) :57500"
"power>25:0"
"op_mode (11 to 11.2) :10289"
"nacelle dir std (<1) :12735"
"windspeed (5 to 13 m/s) :3292"
"v/v_nac (0.9 to 1.1) :3305"
"TI (0.01 to 0.2) :52"
"pitch_dif (<0.05 deg) :649"
"wind shear ws80/ws50 (1 to 1.2):3057"
"pitch_angle (0.065 deg) :898"
"final length:13224"

—— Data reduction log for turbine 5 power dataset 1 (10 minute average) ——

"start length:105336"
"NaN in yaw:1778"
"data set 1 :63557"
"NA in Pair:0"
"wind dir (220 to 280deg) :15277"
"power>25:0"
"op_mode (11 to 11.2) :5852"
"nacelle dir std (<1) :9700"
"windspeed (5 to 13 m/s) :1341"
"v/v_nac (0.9 to 1.1) :840"
"TI (0.01 to 0.2) :6"
"pitch_dif (<0.05 deg) :299"
"wind shear ws80/ws50 (1 to 1.2):1193"
"pitch_angle (0.065 deg) :300"
"final length:5193"

—— Data reduction log for turbine 5 power dataset 2 (2 minute average) ——

"start length:770909"

"NaN in yaw:11330"
"data set 2 :589578"
"NA in Pair:0"
"wind dir (220 to 280deg) :89775"
"power>25:0"
"op_mode (11 to 11.2) :17152"
"nacelle dir std (<1) :9815"
"windspeed (5 to 13 m/s) :4278"
"v/v_nac (0.9 to 1.1) :11902"
"TI (0.01 to 0.2) :566"
"pitch_dif (<0.05 deg) :36"
"wind shear ws80/ws50 (1 to 1.2):6276"
"pitch_angle (0.065 deg) :8009"
"final length:22192"

Data reduction log for turbine 5 power dataset 2 (5 minute average)

"start length:296096"
"NaN in yaw:4551"
"data set 2 :231544"
"NA in Pair:0"
"wind dir (220 to 280deg) :31321"
"power>25:0"
"op_mode (11 to 11.2) :6699"
"nacelle dir std (<1) :6553"
"windspeed (5 to 13 m/s) :1146"
"v/v_nac (0.9 to 1.1) :2358"
"TI (0.01 to 0.2) :26"
"pitch_dif (<0.05 deg) :5"
"wind shear ws80/ws50 (1 to 1.2):1753"
"pitch_angle (0.065 deg) :2056"
"final length:8084"

Data reduction log for turbine 5 power dataset 2 (10 minute average)

"start length:105336"
"NaN in yaw:1778"

```
"data set 2 :83557"
"NA in Pair:0"
"wind dir (220 to 280deg) :7019"
"power>25:0"
"op_mode (11 to 11.2) :3637"
"nacelle dir std (<1) :4596"
"windspeed (5 to 13 m/s) :265"
"v/v_nac (0.9 to 1.1) :393"
"TI (0.01 to 0.2) :5"
"pitch_dif (<0.05 deg) :5"
"wind shear ws80/ws50 (1 to 1.2 ):586"
"pitch_angle (0.065 deg) :1115"
"final length:2380"
```

B.2 Turbine 6

Data reduction log for turbine 6 loads (2 minute average)

```
"start length:406569"
"NaN in yaw:6416"
"data set 1 :200151"
"NA in Pair:0"
"NA in Medge_C1:25244"
"NA in Mflat_C1:0"
"NA in Medge_C3:0"
"NA in Mflat_C3:0"
"wind dir (110 to 140 and 200 to 250deg) :0"
"power>25:12178"
"op_mode (11 to 11.2) :75388"
"nacelle dir std (<1) :1449"
"windspeed (5 to 13 m/s) :9294"
"v/v_nac (0.9 to 1.1) :11853"
"TI (0.01 to 0.2) :949"
"pitch_dif (<0.05 deg) :29137"
"wind shear ws80/ws50 (1 to 1.2 ):7182"
"pitch_angle (0.1 deg) :0"
"final length:27328"
```

Data reduction log for turbine 6 loads (5 minute average)

"start length:136504"
"NaN in yaw:2072"
"data set 1 :64430"
"NA in Pair:0"
"NA in Medge_C1:8228"
"NA in Mflat_C1:0"
"NA in Medge_C3:0"
"NA in Mflat_C3:0"
"wind dir (110 to 140 and 200 to 250deg) :0"
"power>25:4678"
"op_mode (11 to 11.2) :27604"
"nacelle dir std (<1) :1312"
"windspeed (5 to 13 m/s) :2996"
"v/v_nac (0.9 to 1.1) :2332"
"TI (0.01 to 0.2) :84"
"pitch_dif (<0.05 deg) :10552"
"wind shear ws80/ws50 (1 to 1.2):2324"
"pitch_angle (0.1 deg) :0"
"final length:9892"

Data reduction log for turbine 6 loads (10 minute average)

"start length:82246"
"NaN in yaw:1619"
"data set 1 :34425"
"NA in Pair:0"
"NA in Medge_C1:10750"
"NA in Mflat_C1:0"
"NA in Medge_C3:0"
"NA in Mflat_C3:0"
"wind dir (110 to 140 and 200 to 250deg) :0"
"power>25:1731"
"op_mode (11 to 11.2) :19307"
"nacelle dir std (<1) :6485"
"windspeed (5 to 13 m/s) :633"
"v/v_nac (0.9 to 1.1) :418"
"TI (0.01 to 0.2) :13"

```
"pitch_dif (<0.05 deg) :2297"
"wind shear ws80/ws50 (1 to 1.2 ):886"
"pitch_angle (0.1 deg) :0"
"final length:3682"
```

C

Data reduction figures

C.1 Turbine 5

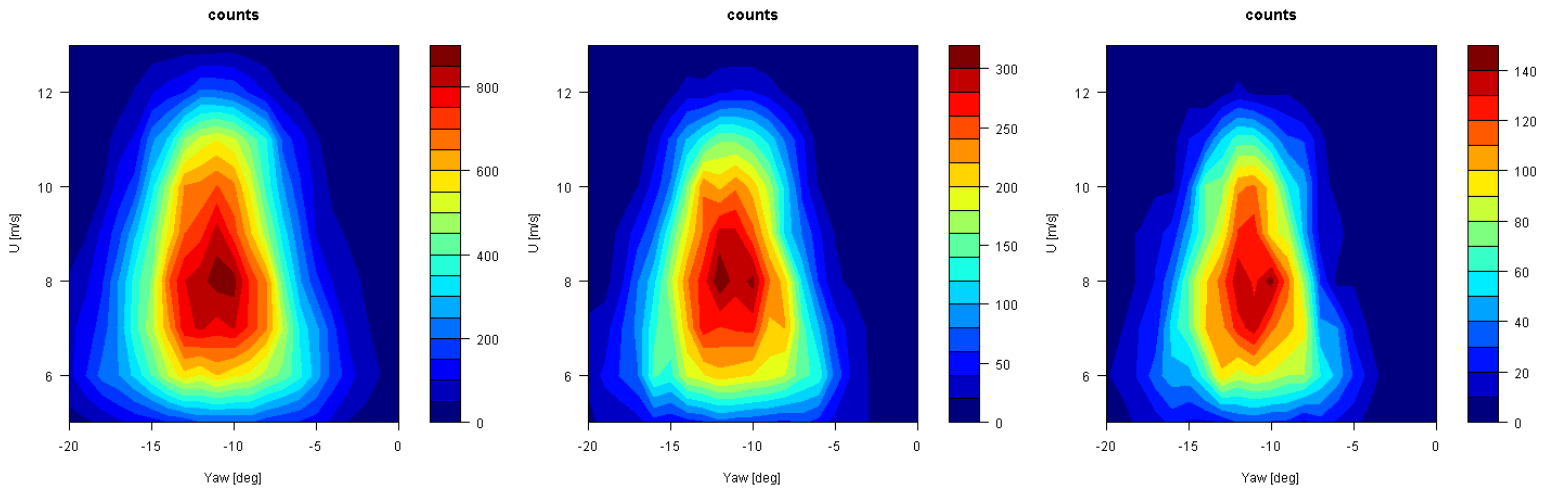

(a) 2 minute average, set 1

(b) 5 minute average, set 1

(c) 10 minute average, set 1

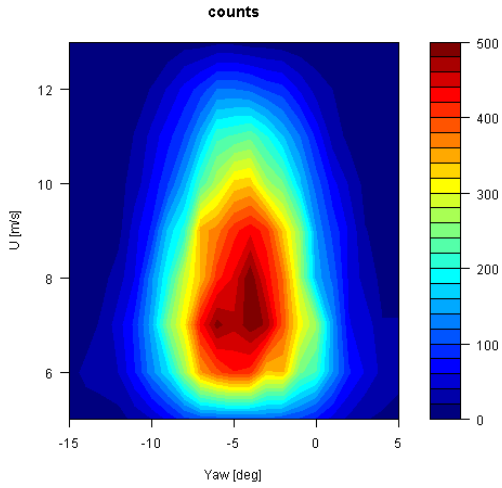

(d) 2 minute average, set 2

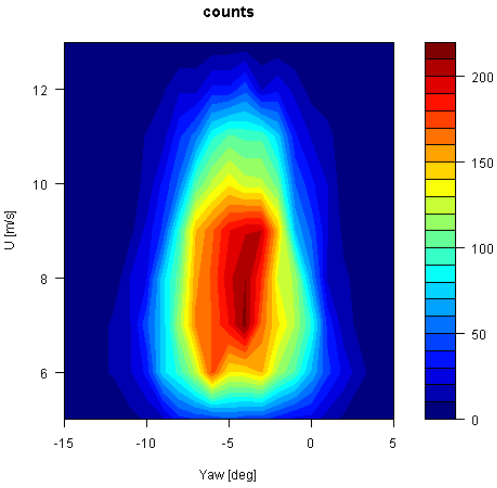

(e) 5 minute average, set 2

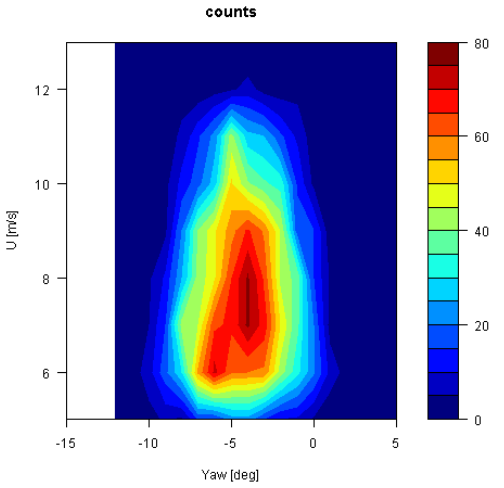

(f) 10 minute average, set 2

Figure C.1: Number of samples for data set 1 (above) and 2 (below), turbine 5

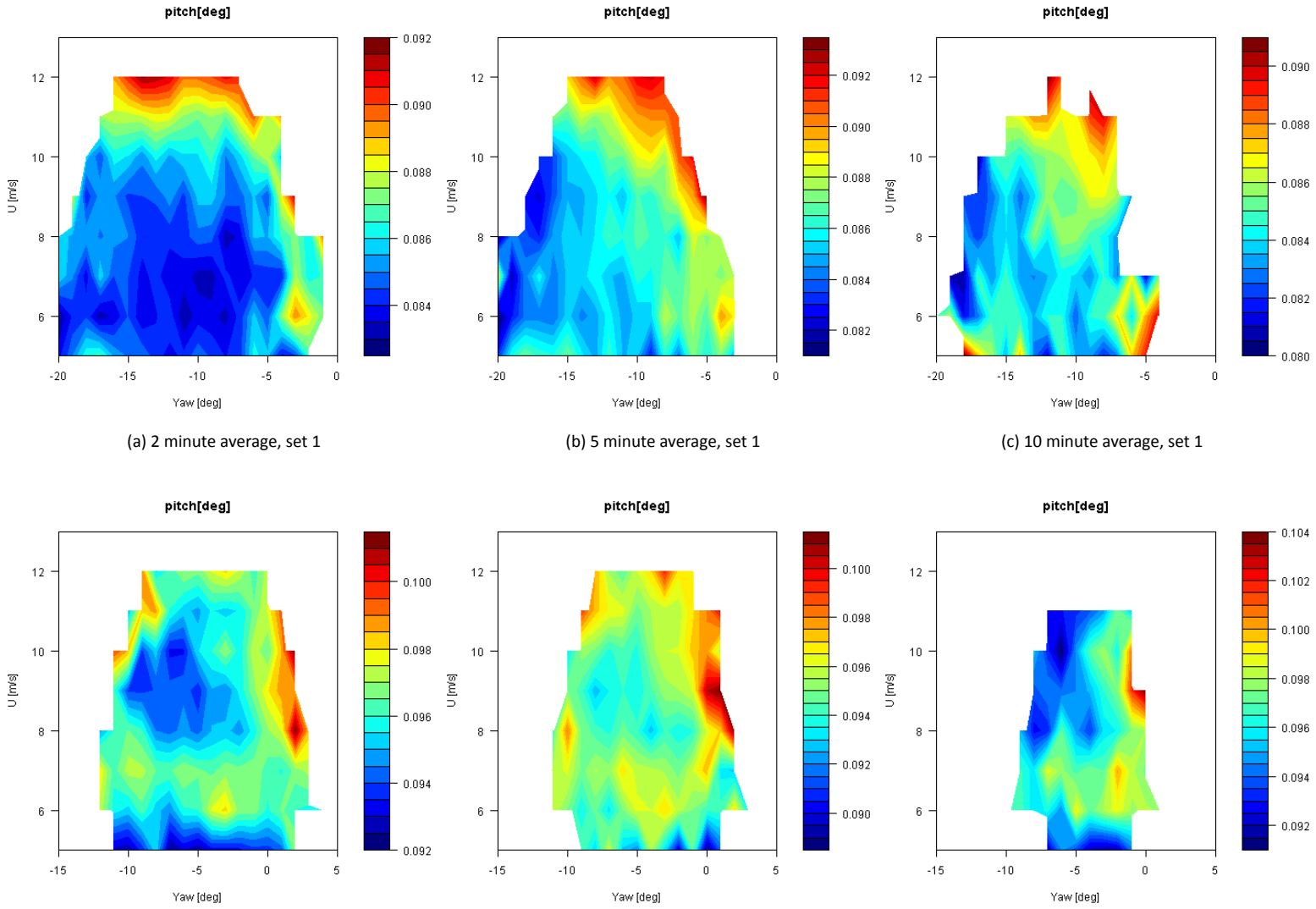

(a) 2 minute average, set 1

(b) 5 minute average, set 1

(c) 10 minute average, set 1

(d) 2 minute average, set 2

(e) 5 minute average, set 2

(f) 10 minute average, set 2

Figure C.2: Pitch angles for data set 1 (above) and 2 (below), turbine 5

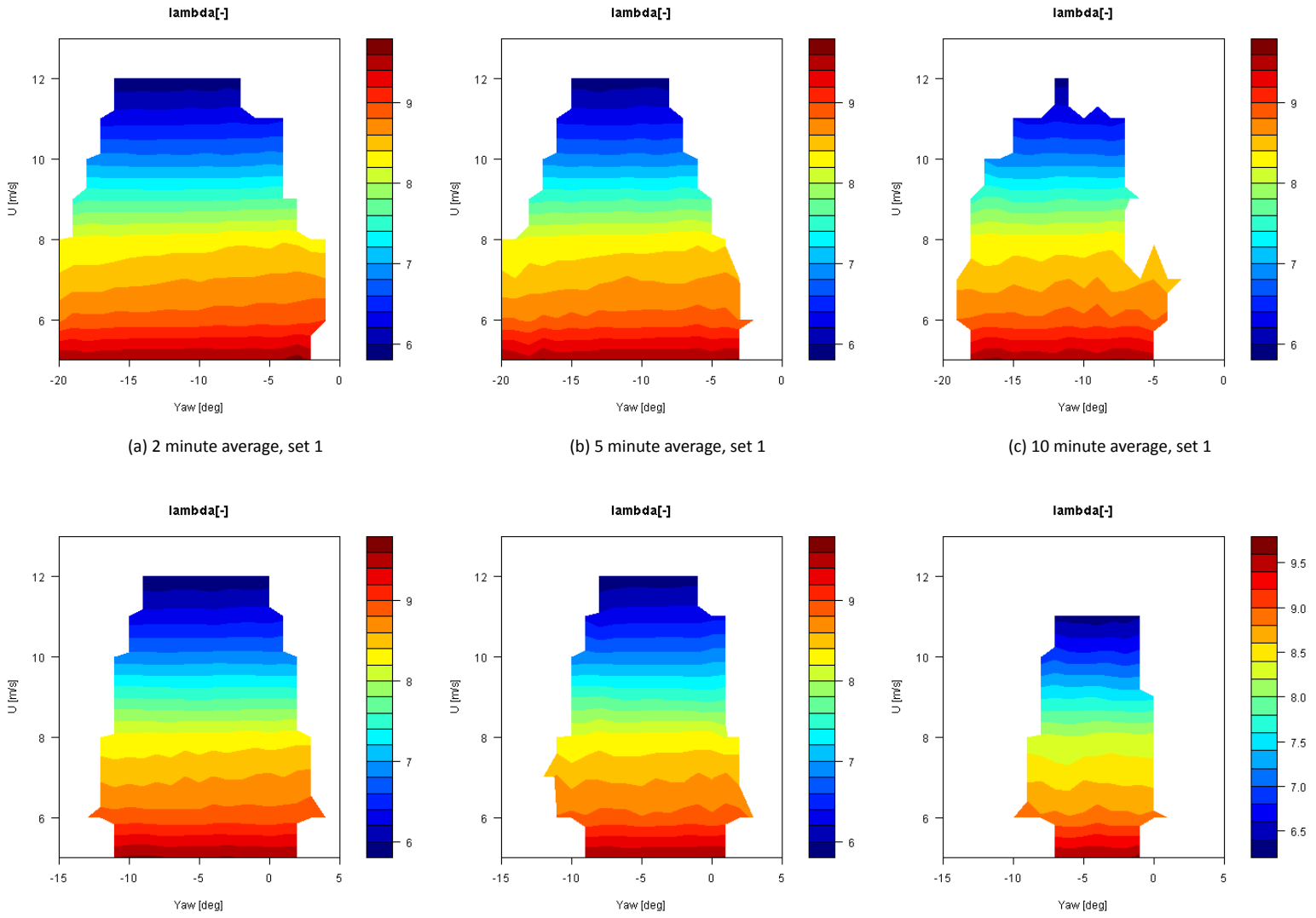

(a) 2 minute average, set 1

(b) 5 minute average, set 1

(c) 10 minute average, set 1

(d) 2 minute average, set 2

(e) 5 minute average, set 2

(f) 10 minute average, set 2

Figure C.3: Tip speed ratios for data set 1 (above) and 2 (below), turbine 5

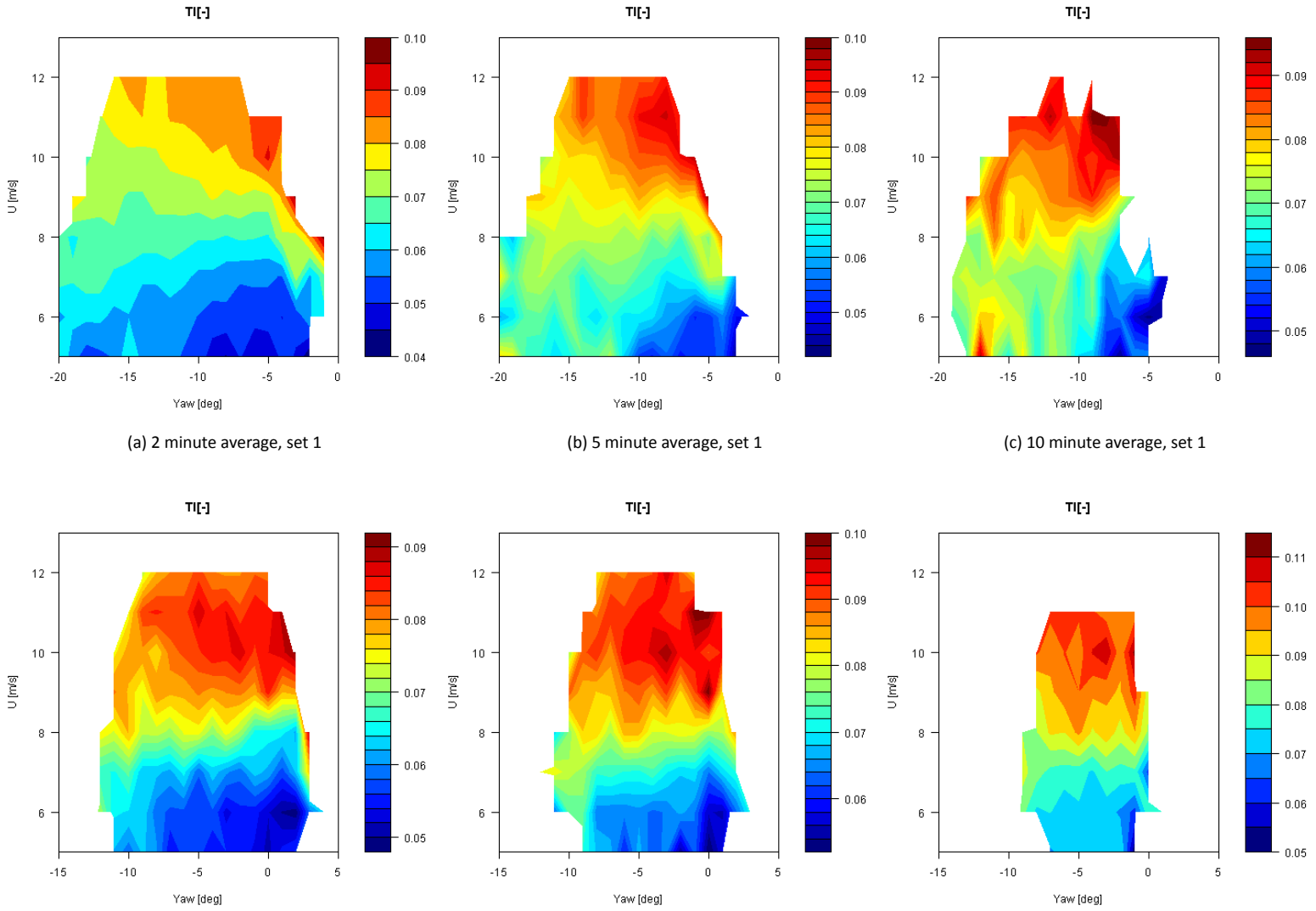

(a) 2 minute average, set 1 (b) 5 minute average, set 1 (c) 10 minute average, set 1

(d) 2 minute average, set 2 (e) 5 minute average, set 2 (f) 10 minute average, set 2

Figure C.4: Turbulence intensity for data set 1 (above) and 2 (below), turbine 5

C.2 Turbine 6

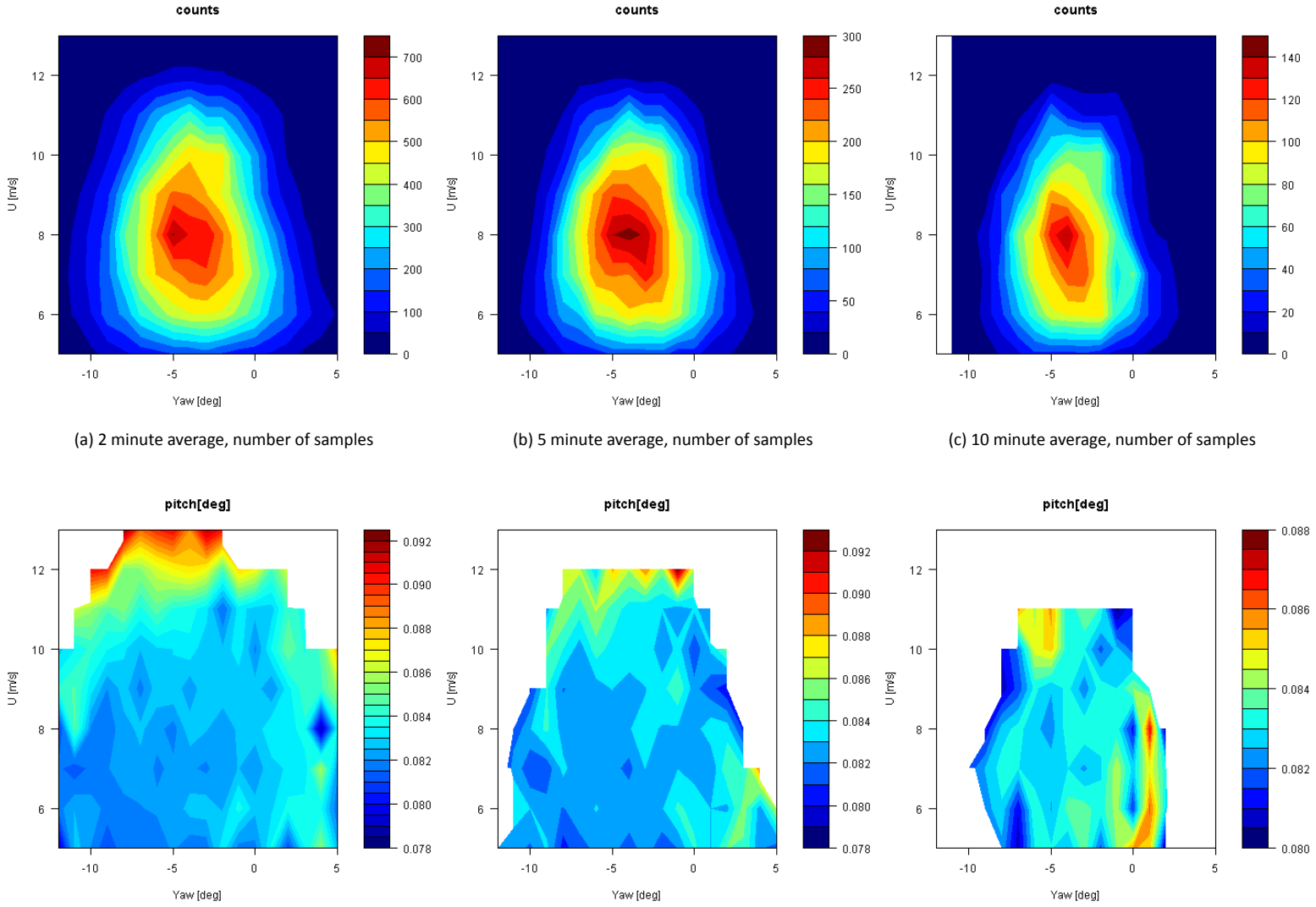

(a) 2 minute average, number of samples

(b) 5 minute average, number of samples

(c) 10 minute average, number of samples

(d) 2 minute average, pitch angle

(e) 5 minute average, pitch angle

(f) 10 minute average, pitch angle

Figure C.5: Number of samples (above) and pitch angle (below), turbine 6

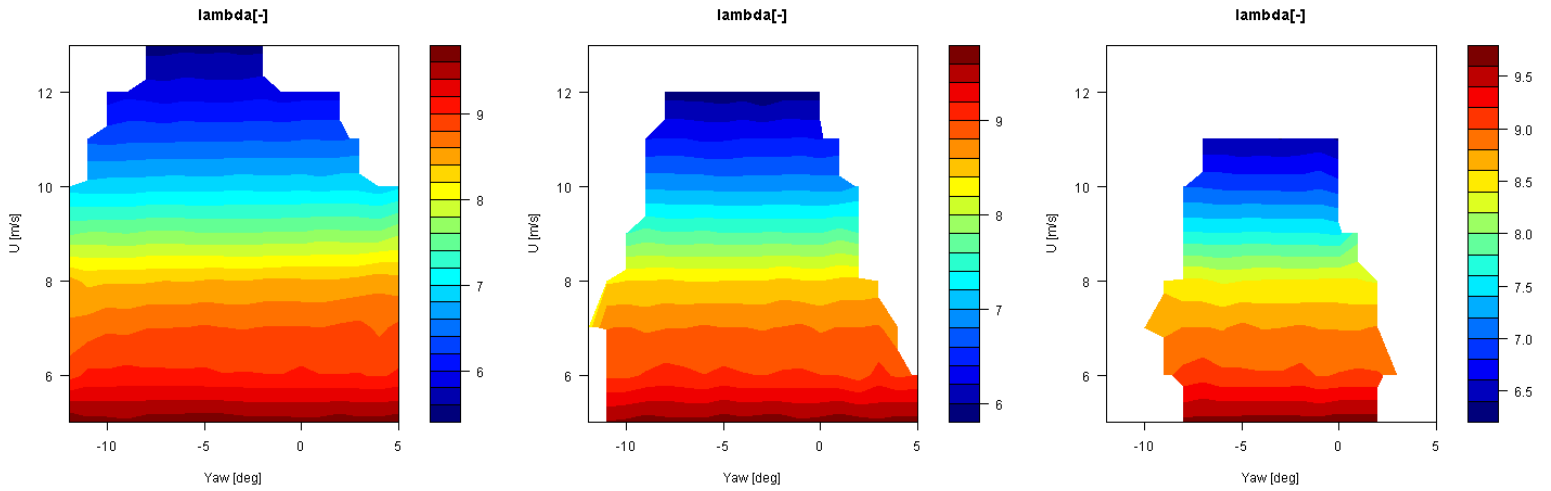

(a) 2 minute average, tip speed ratio

(b) 5 minute average, tip speed ratio

(c) 10 minute average, tip speed ratio

(d) 2 minute average, turbulence intensity

(e) 5 minute average, turbulence intensity

(f) 10 minute average, turbulence intensity

Figure C.6: Tip speed ratio (above) and turbulence intensity (below), turbine 6

D

Beddoes Leishman implementation

The Beddoes Leishman dynamic stall model essentially consists of four subsystems:

1. Attached flow model, including an impulsive component and circulatory (shed vorticity) component.
2. A trailing edge separation module to include the effect of the dynamic separation point position.
3. A leading edge separation module to predict dynamic stall onset. Leading edge separation lag is included.
4. A vortex module to calculate the possible vortex induced aerodynamic forces.

These four sub-models are connected in an open loop system, where output from one model serves as input for the next. More details can be found in [11, 12]. The specific implementation in the `ECN Aero-Module` is based on the work described in [18], [9] and [3]. This implementation is briefly described below.

- Wind reference frame
  As suggested in [3] the wind reference frame is used instead of the body fixed reference frame (normal and tangential force coefficients). For low angles of attack the difference obviously is small. The only exception lies in the vortex lift, which is calculated in terms of C_n and decomposed in the wind reference frame afterwards.
- Angle of attack
  The angles of attack are modified to ensure the angle of attack is limited between -90° and 90°:

$$\begin{aligned} \alpha_{mod} &= \alpha - 180 \quad \alpha > +90 \\ \alpha_{mod} &= \alpha + 180 \quad \alpha < -90 \quad , \end{aligned} \tag{D.1}$$

with

α_{mod}	[°]	Modified angle of attack for usage in Beddoes-Leishman model
α	[°]	Original angle of attack

In addition to this a fading function ($\cos^2 \alpha$) is applied to angle of attack variations that are fed into the model. This in order to avoid queer results at high angles of attack.

- Parameters
  Several parameters are used throughout the model. Some depend on airfoil shape, most of them are time constants. The values used in the `ECN Aero-Module` are currently fixed and given in Table D.1.

Table D.1: Implemented Beddoes-Leishmann parameter values as defined in [11, 12]

A_1	A_2	b_1	b_2	K_α	T_p	T_f	T_v	T_{vl}	A_{cd}
0.3	0.7	0.14	0.53	0.75	1.5	5	6	5	0.13

- Shed vorticity
  As mentioned, the influence of shed vorticity on the profile aerodynamics is included in the Beddoes-Leishmann model. Since this effect is accounted for by `AWSM` as well, this contribution is excluded for `AWSM` simulations by not correcting the equivalent angle of attack with deficiency functions.
- Lift curve slope
  The lift curve slope is taken as 2π throughout the module for non-cylindrical shapes ($t/c < 0.8$). An exception lies in the circulatory lift component. To account for the influence of shed vorticity in separated flow conditions, it can be argued to use the lift history rather than angle of attack history. For a better prediction of this effect, the local lift curve slope is used to correct the angle of attack history for calculation of the deficiency functions:

$$\Delta\alpha_{cor} = \Delta\alpha \frac{\partial Cl/\partial\alpha_{loc}}{2\pi} \quad , \tag{D.2}$$

with

$\Delta\alpha$	[rad]	Angle of attack difference with previous time step
$\Delta\alpha_{cor}$	[rad]	Corrected angle of attack difference with previous time step
$\partial Cl/\partial\alpha_{loc}$	[rad^{-1}]	Local lift curve slope.

- Leading edge stall criterium
  As suggested in [18], the occurrence of leading edge stall is determined by monitoring the force coefficient compared to its maximum value. Instead of the maximum normal force however the maximum lift force coefficient is taken. The criterium triggers vortex position tracking, which influences the magnitude of the vortex induced force and moment.

– Moment coefficient

The model contribution to the dynamic moment coefficient originate from the impulsive and vortex module:

$$\Delta Cm = Cm_i + Cm_v \quad , \tag{D.3}$$

with

ΔCm	[-]	Dynamic addition to static moment coefficient (positive nose up)
Cm_i	[-]	Dynamic addition due to impulsive lift
Cm_v	[-]	Dynamic addition due to vortex lift.

As suggested in [3] the impulsive contribution can be estimated by adding the impulsive lift:

$$Cm_i = 0.25 Cl_i \quad , \tag{D.4}$$

with

Cl_i	[-]	Impulsive lift coefficient.

The addition due to the vortex module depends on the vortex position:

$$Cm_v = -0.2\big(1 - \cos(\pi\tau_v / T_{vl})\big) Cl_v \quad , \tag{D.5}$$

with

τ_v	[-]	Nondimensional vortex time
Cl_v	[-]	Vortex lift contribution.

– Drag

The model contribution to the dynamic drag coefficient originates from several modules:

$$\Delta Cd = Cm_i + Cd_v \quad , \tag{D.6}$$

with

ΔCd	[-]	Dynamic addition to static drag coefficient
Cd_i	[-]	Dynamic addition due to the shed wake induced drag
Cd_s	[-]	The change in drag due to the separation point position being different from its static position
Cd_v	[-]	Dynamic addition due to vortex induced normal force.

The shed wake induced drag is calculated by means of

$$Cd_i = \sin(\alpha - \alpha_E) Cl_f \quad , \tag{D.7}$$

with

α	[°]	Angle of attack
α_E	[°]	Angle of attack corrected for shed wake effect
Cl_f	[-]	Lift coefficient corrected for non-linear trailing edge separation.

The separation drag is calculated by means of

$$Cd_s = A_{cd}(Cl - Cl_f) \quad , \tag{D.8}$$

with

A_{cd}	[-]	Constant taken from Table D.1
Cl	[-]	Static lift coefficient.

The vortex drag is calculated by means of decomposing the vortex induced normal force in drag direction.

A detailed comparison of the performance of different various dynamic stall models can be found in [9].

E

Validation of calculated levels in axial flow

To make sure that that the flow physics is well approximated for axial inflow conditions, the computed absolute value results are compared in Figure E.1. The trends with tip speed ratio $lambda$ show a satisfactory agreement for both the BEM and AWSM results. The overprediction of power and axial force for the MEXICO rotor compared to this experiment is not a major concern; this in agreement with a wide variety of design codes and CFD codes as reported in IEA Task 29 Mexnex(t) [21]. As expected, the differences between BEM and AWSM are small for axial flow conditions.

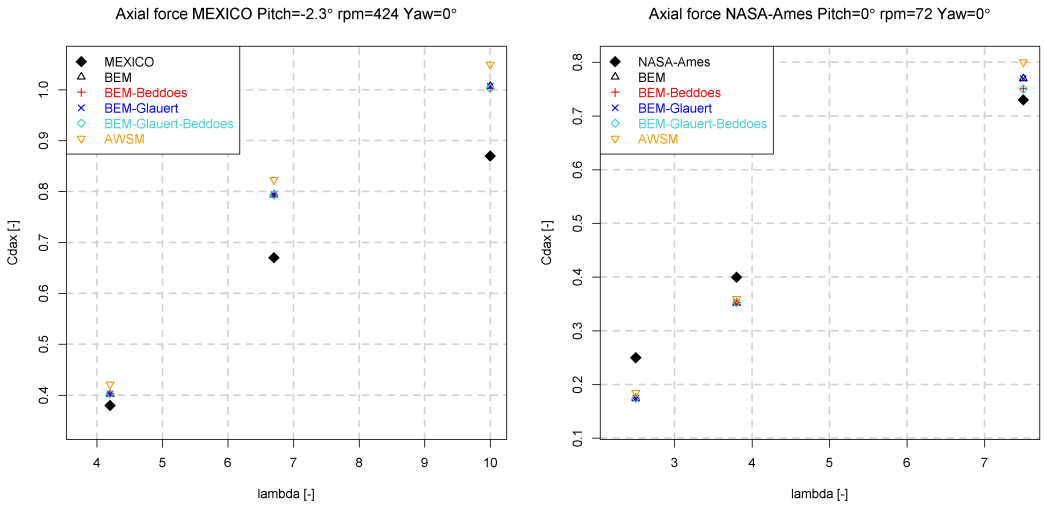

(a) MEXICO, axial force

(b) Nasa-Ames, axial force

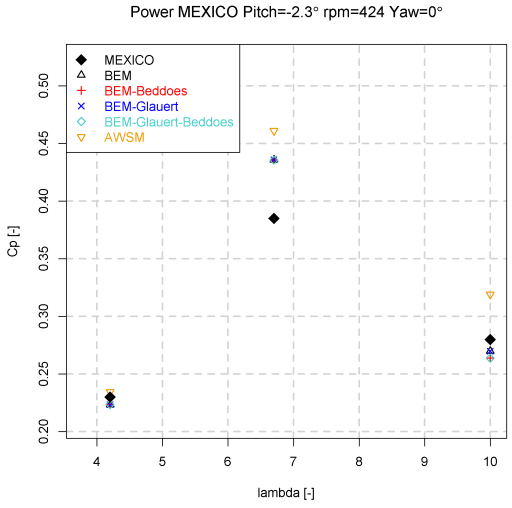

(c) MEXICO, power

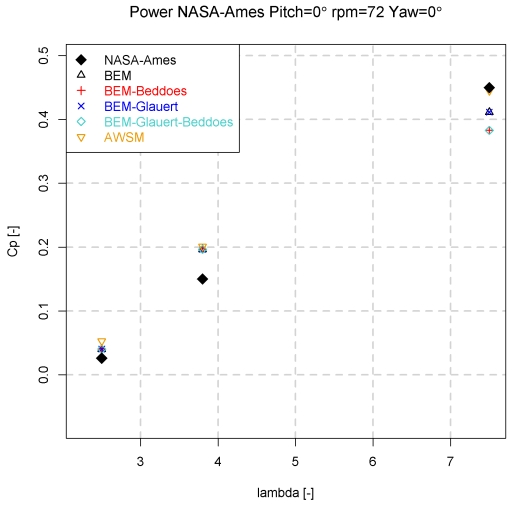

(d) Nasa-Ames, power

Figure E.1: Calculated and measured power and axial force coefficients for MEXICO and Nasa-Ames experiment

ECN
Westerduinweg 3
1755 LE Petten
The Netherlands

P.O. Box 1
1755 ZG Petten
The Netherlands

T +31 88 515 4949
F +31 88 515 8338
info@ecn.nl
www.ecn.nl